International Journal of Machine Tools & Manufacture 183 (2022) 103964

Contents lists available at ScienceDirect

International Journal of Machine Tools and Manufacture

journal homepage: www.elsevier.com/locate/ijmactool

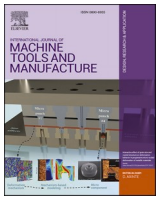

Review Article

What micro-mechanical testing can reveal about machining processes

Dragos Axinte [a], Han Huang [b], Jiwang Yan [c], Zhirong Liao [a,*]

[a] Faculty of Engineering, University of Nottingham, UK
[b] School of Mechanical & Mining Engineering, University of Queensland, Australia
[c] Faculty of Science and Technology, Keio University, Japan

ARTICLE INFO

Keywords:
Micro-mechanical testing
Indentation
Scratching
Micro-machining
Micro-pillar
Material removal mechanism

ABSTRACT

For many years, the machining community has dedicated significant efforts to investigate the microscopic scale level phenomena during the material removal process. On one hand much research has been carried out in relation to workpiece surface integrity after machining and the methods for its study. On the other hand, many studies have been dedicated to replicate machining conditions at microscopic scales using high resolution setups. Although these two topics seem to be little related, there is an opportunity of the machining community to take the advantage of the advanced testing/investigation setups that enable these two strands of research to be performed at very high resolution and repeatability, thus giving new pathways for research in this field. Here we are flagging up to the community the research opportunities offered by micro-mechanical testing that can be performed using in-situ scanning electron microscopes (SEM) or other high-resolution imaging instruments. As such, this review paper discusses the recent research advances in using in-situ micro-mechanical testing for: *(i)* understanding the phenomena occurring in the workpiece (sub) surfaces after machining operation by performing very high resolution micro-mechanical testing (e.g. compression/bending of micro-pillars/beams) within particular zones of machined superficial layers; *(ii)* studying the material removal mechanisms at micrometric level using common indenters or dedicated edges to understand how the workpiece materials (e.g. groups/single grains) react to cutting conditions. Finally, we comment on possible future research topics using micro-mechanical testing in-situ in high resolution imaging instruments and how this could help to advance the understanding of machining processes.

1. Introduction

With the intense thermo-mechanical loads occurring in machining there are a set of multiple scale (i.e., from macro to micro level) material deformation/transformation mechanisms at tool-workpiece interface, aspects which captured the attention of the research community for decades [1,2]. While studies directed to observe/visualise the mechanisms (e.g. material flow patterns, chip formation) of cutting directly on machine tool setups were early reported [3,4], the more recent updates of these experimental methods by use of more advanced instrumentations still provide information that could be considered at macro-level. Of course, such tests can be followed by more in-depth post-mortem analysis (Scanning Electron Microscopy - SEM, Transmission Electron Microscopy - TEM) on both the workpiece [5] and tool surfaces [6] to derive/infer aspect of macro-phenomena occurring during the process.

As such, over the years, the machining research community has been developing dedicated, and every time more instrumented, experimental setups with 1–3 linear axis (which can reach high level of instrumentation [7]), that usually try to replicate the "on-machine" conditions while allowing the addition of key sensors (e.g. high speed camera/-thermal imaging) to enable the elucidation, in much more detail, different aspects of the machining process (e.g. material deformation, cracking), as shown in Fig. 1. However, being carried out in conditions, somehow, similar to those of real machine tool setups, in these studies the workpiece response to cutting is still at macro-level while, as mentioned above, some post-mortem workpiece material analysis could be performed with a higher level of confidence as some disturbances caused by the real machine setups (e.g. vibration) can be eliminated and, thus, the cutting phenomena can be studied in more detail [8].

To further deepen the studies of the material removal mechanisms, some unique experiments (e.g. split Hopkinson bar [9], quick stop [10], pendulum [11], ultramicrotomy [12], etc.) were developed at early stages of research in machining technology that started from the basic

* Corresponding author.
E-mail address: Zhirong.Liao@nottingham.ac.uk (Z. Liao).

https://doi.org/10.1016/j.ijmachtools.2022.103964
Received 16 August 2022; Received in revised form 1 October 2022; Accepted 19 October 2022
Available online 22 October 2022

principles of the process. These approaches offered guidance to enter the remit of tests on which carefully prepared cutting edges/indenters are moved along simple trajectories while observing the material being removed as well as machined surface being generated. Such experiments usually make use of simple setups, e.g., linear/rotary stages on which the cutting edge/indenter is presented to the workpiece in very precise mode, equipped with advanced sensorial systems (e.g., force, temperature, etc.). Although the study of machined surface could be carried out at different scales (e.g., macro: dedicated machine-like setups/simplified tests like pendulum based cutting [13]; meso: scratch tests [14]) it could be commented that, in these cases, the cutting mechanisms are observed at meso-level (e.g. tens of microns covering multi-grain areas of the workpiece material).

Nevertheless, in the last decades the material research community has been making use of advanced setups that, within, "in-situ", advanced microscopy equipment (e.g., SEM), can perform mechanical testing (as low and high strain rates) at micrometric level. These tests offer, on one hand, the possibility to observe in-situ high resolution microscopes the material failure/deformation mechanisms under different testing setups (e.g., compression, bending, facture toughness, scratch/abrasion) while also allowing the analysis on some critical mechanical properties of the workpiece materials (e.g., nano-hardness, strains) at micro-level. This approach is usually denominated as *In-Situ Micro-Mechanical Testing* and, it could be said, that the ability to perform highly accurate tests are driven by some specialist equipment developers (e.g., Alemnis). These special techniques now are becoming popular to the material scientists who have been pushing the boundaries of mechanical characterisation of various materials (from diamond to organic materials) to micron, and, in some instances, sub-micron level.

In the recent years, there have been some steps in using these *micro-mechanics* facilities to perform "cutting tests" in-situ SEM or other imaging systems to enable the understanding of the related governing phenomena at micro-level. Although it appears that there is a research appetite in the machining community for such approaches, this paper intends to present a structured map of what these state-of-the-art micro-mechanical testing instrumentations/methods can offer in studying interesting research avenues and novel scientific point of view related to this topic.

As such, it is felt that firstly, there is a need to shortly present the equipment that enable *in-situ micro-mechanical* studies. While there are not many commercially available instrumentation for this, the basic principles are: miniaturised linear stages (commonly piezoelectrically actuated) with <1 nm positioning resolution capable to cover a wide range of displacement strain rates (e.g., 10^{-3}/s – 10^{3}/s in nano-indentation), equipped with 1D/3D force sensors (uN resolution), are employed under a very high magnification microscopes (usually SEM) to provide highly controlled relative motion between an indenter and a workpiece (Fig. 2). Of course, when using these devices in-situ SEM, there is a need that their dimensions are small enough to fit into the vacuum chamber of such microscopes. As such, these systems enable the observation (via video recording, usually tens of frames per second for SEM depending on the scanning resolution) of the contact zone between the indenter and workpiece. The piezoelectric sensors/actuators allow the load application in static and dynamic modes. Further facilities can be added to the system such as high-temperature sample heating module. The accompanying software can yield various outputs (e.g., load-displacement curves) while allowing the input on critical corrections (e.g. stiffness of the system equipped with a particular indenter), etc.

On the other hand, although some materials properties (e.g., hardness, residual stress) can be already achieved through conventional materials characterizations, these high precision systems for in-situ micro-mechanical testing can offer to the machining community unique avenues of research as follows (Fig. 3): *i)* mimic/replicate machining operations at micrometric level and in observant medium; this can be done using off-the-shelf or close-to-real cutting edges to perform indentations/scratches/ploughing/shearing of the workpiece material to replicate some of the mechanisms that are involved in the cutting process; *ii)* study the workpiece material mechanical deformation/properties at crystallographic level and the aspects of chip formation at microscopic level when a tool removes material; this can be done by preparing pillars/beams in very precise locations in the superficial layer affect by machining by use of Focused Ion Beam (FIB) followed by mechanical testing (e.g. compression, bending) respectively in static/dynamic mode.

As such, the context set by this review, the micro-mechanical studies are needed to: *i)* capture the specifics of cutting at micro-level (when the instrumentation is used to mimic a cutting process) as tool/indented is faces anisotropies of the material (e.g. different grain orientations); or *ii)* map the variation of material properties under the machined surface (when the instrumentation is used as a material testing method).

2. Replicating of machining processes at micro-level

Micro-scale phenomena that occur during the machining process is of importance to understand the fundamental mechanism of machining. As mentioned above, among common methods to "replicate" cutting processes using micro-mechanics testing systems could be mentioned: scratching (with off-the-shelf indenters) and cutting (with geometry customised tips).

2.1. Fundamental micro-mechanics for scratching

2.1.1. Theoretical background

Indentation mechanics has taken a central place in the understanding of the intrinsic mechanisms of deformation and removal involved in a machining process with individual tool-workpiece contacts at micro-

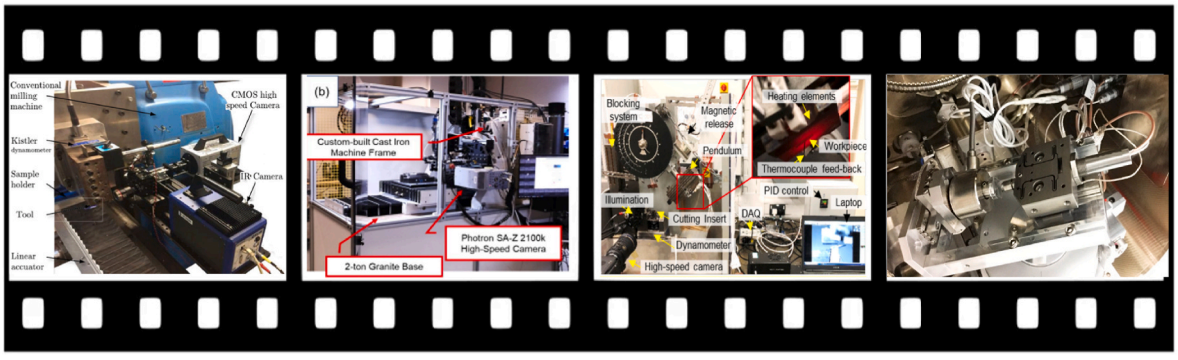

Fig. 1. An simplified overview of machining testing: from on-machine [15] (a), specialist "machine-like" setup [7] (b), simplified pendulum-base cutting [16] (c) to in-situ SEM testing [17] (d).

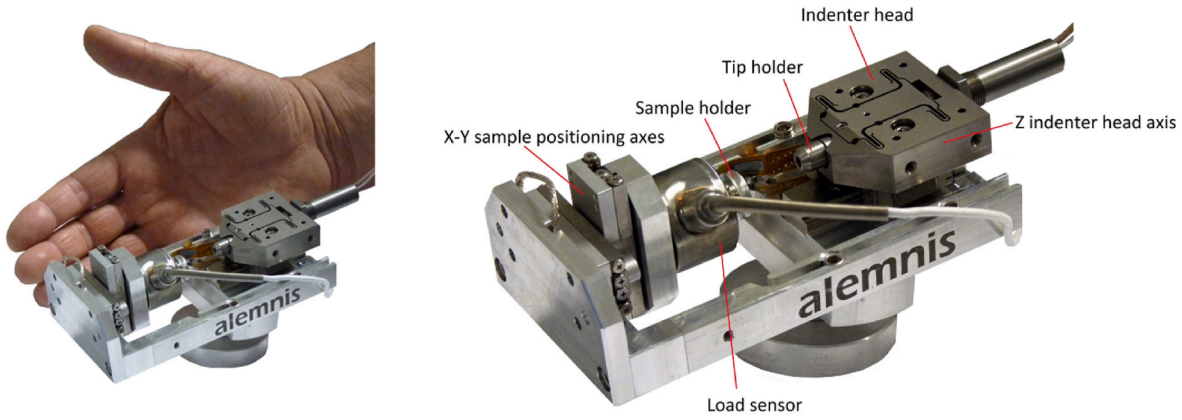

Fig. 2. An example of a commercially available system for in-situ testing for micro-mechanics evaluation [17].

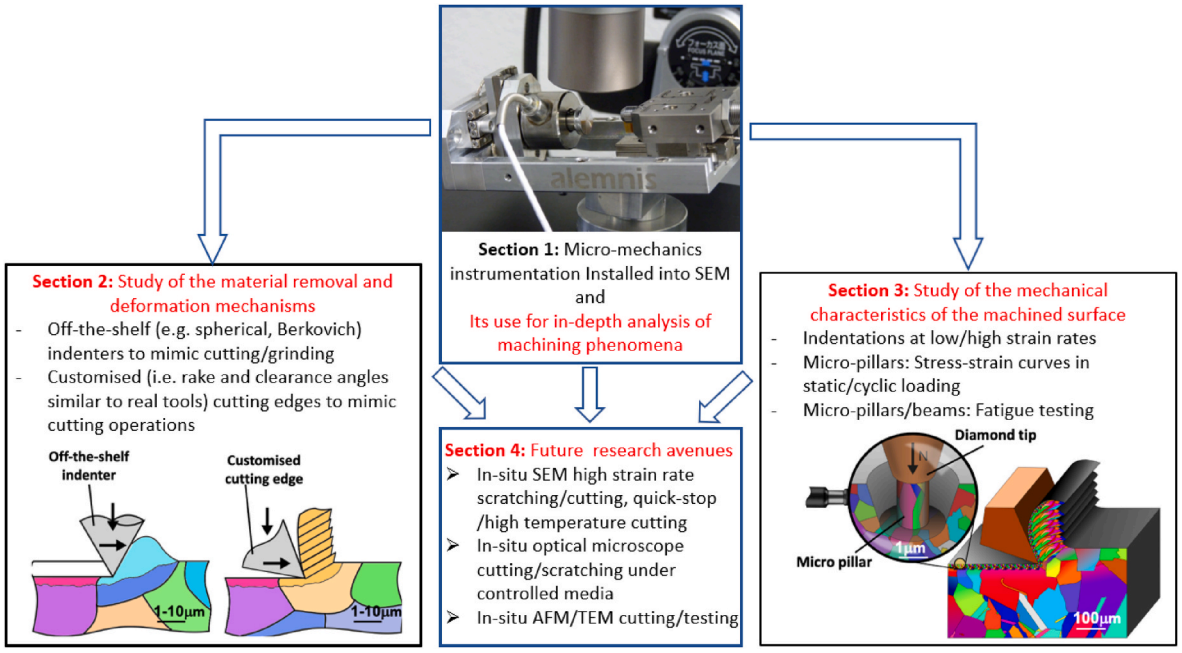

Fig. 3. A summary of the key research directions that in-situ micro-mechanical testing instrumentations/methods can offer to the machining research.

level. With the theory of contact mechanics, the deformation patterns of a work material, or its fracture modes if concerning a brittle solid, under the impression of a hard indenter can be characterized, which are related to the axial load of the tool used, as well microstructure and mechanical properties of the material. For both ductile and brittle materials, a plastic zone that is induced under an axial load P at the normal direction can be assumed to have a hemispherical shape.

The applied axial load P leaves an impression of half-diagonal "a" for a pyramid indenter or radius "a" for a conical indenter, under which is a hemispherical plastic zone of radius "b". For a ductile material, a plastically deformed zone is generated, as displayed in Fig. 4(a). The dimension a is determined by material hardness H and load P [18],

$$P/\alpha a^2 = H \tag{1}$$

With α an indenter shape factor, 2 for Vickers and p for conical. In a brittle solid, a median crack "c" will be induced if the stress intensity is sufficiently great [19], as shown in Fig. 4(b), and there exists a relation between P, mechanical properties, and c [20,21]

$$P/c^{3/2} \sim (H/E)^{1/2}T \tag{2}$$

where H, E and T are hardness, elastic modulus, and fracture toughness,

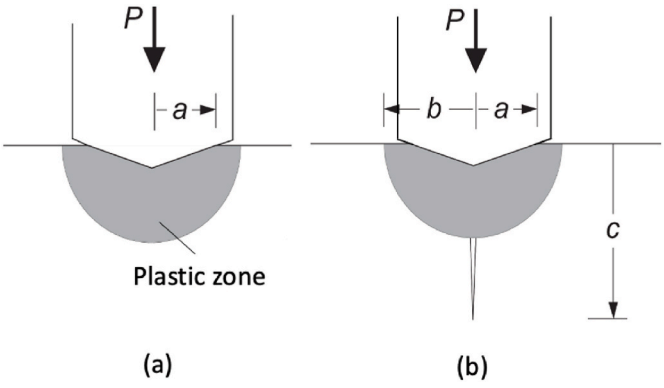

Fig. 4. Indentation induced damage in (a) ductile and (b) brittle materials. An indenter at normal load P leaves impression of half-diagonal a surrounded by hemispherical plastic zone of radius b and can produce a crack of length c in a brittle solid.

respectively. For coarse-grained heterogeneous brittle materials, the stress intensity that generates microcracks at weak grains or grain boundaries is different from that when generating median cracks, which is related to grain size and the toughness pertaining to the short-crack region of an R-curve that relates crack growth resistance to crack propagation [22].

It should be note that, the indentation mechanics does not take account for the effect of translational loading that is superposed onto normal loading in the cutting and abrasive processing of a material. Therefore, in recent years the scratch-based micro-mechanical tests are often used for analysing machining processes and quantifying associated material removal mechanism [14]. Fig. 5 shows the basic patterns of deformation or/and fracture of a material induced by scratching at microscale. Those patterns have similar forms to the respective indentation induced damage modes but caused by imposing a tangential load onto the indentation axial load [14,23]. In Fig. 5(a), scratching of a ductile material generates a plastic zone underneath the scratched path, pileups are often seen along the side stringers of the scratched groove. Such a deformation mode can also be seen in the scratching of a brittle material where penetration depth is very shallow, and contacts are in the subthreshold region where cracks are suppressed. Material removal in Fig. 5(a) is principally via extrusion, but shear removal can happen if the indenter tip is sufficiently sharp. In the brittle region of scratching shown in Fig. 5(b), trailing radial (R), median (M) and lateral (L) cracks are induced when a relatively sharp indenter is used, while intermittent cone (C) cracks are generated with the use of a blunter indenter [22]. The damage patterns are often observed in the scratching of highly brittle/hard single crystals and glasses, showing apparent influence of indenter size and geometry [24]. In the scratching of polycrystal hard/brittle solids, microcracks (μC) and lateral cracks are generated along the grain boundaries of their granular microstructure, which is particularly true for course grained materials, as shown in Fig. 5(c) [22].

2.1.2. Threshold of ductile-to-brittle

In the machining of brittle materials, a threshold of cutting depth or load exists below which ductile removal prevails [25,26]. Estimation of the threshold often used Bifano-Dow-Scattergood (BDS) model in the machining world that was developed based on the indentation micro-mechanics [24]. The derivation of BDS model had an error, which was recently amended. In the amended BDS model [27], the plastic zone is determined by b, not a; however, b can be approximately expressed as a function of a [19],

$$b \sim a\,(E/H)^{1/2} \tag{3}$$

Setting the critical value of a for crack initiation equals that of c, i.e., $a_c = c_c$, and cancelling P in Eqs. (1) and (2) gives a threshold of the impressed area that can be used to suppress crack initiation in machining,

$$a_c \sim (H/E)(T/H)^2 \tag{4}$$

If the critical depth of cut d_c is scaled with b, the combination of Eqs. (3) and (4) gives

$$d_c = \lambda\,(H/E)^{1/2}(T/H)^2 \tag{5}$$

with $\lambda = 8.7$ that is determined using brittle solids with E/H values in between 13 and 17 [27]. Equation (4) can only be used as a rough guide for ductile region machining of brittle materials because there are uncertainties in a variety of geometrical and materials parameters. For a brittle polycrystal solid, the stress intensity for cracking and determination of fracture roughness is affected by the microstructure of the brittle material, and its detailed description can be found elsewhere [22]. As described earlier, with indentation the frictional component is not taken into consideration for determining d_c. A more accurate approach is to determine the d_c value using instrumented scratching.

Two typical examples are shown in Figs. 6 and 7, demonstrating how to find the ductile-to-brittle transition load or penetration depth of GaAs brittle single crystal using the scratching method. Fig. 6(a) presents a SEM image of the scratch on GaAs using a Berkovich indenter of tip radius of 200 nm with a ramping load, displaying radial cracks that were induced along the groove edge at load of above 30 mN (the corresponding depth can be found from the load-displacement curve if needed). When using a 5 μm conical indenter that is much blunter than the Berkovich tip, no apparent penetration occurred in the early stage of scratching, the transition period of ductile to brittle is very short, and many cracks were generated in the bottom of the groove, as shown in Fig. 6(b). Fig. 7 presents cross-sectional TEM images of the scratches made using various constant normal loads with a 3 μm conical indenter. No cracks are observed for the subthreshold scratching at loads of below 6 mN, but a large median crack is found in the sublayer of scratch made

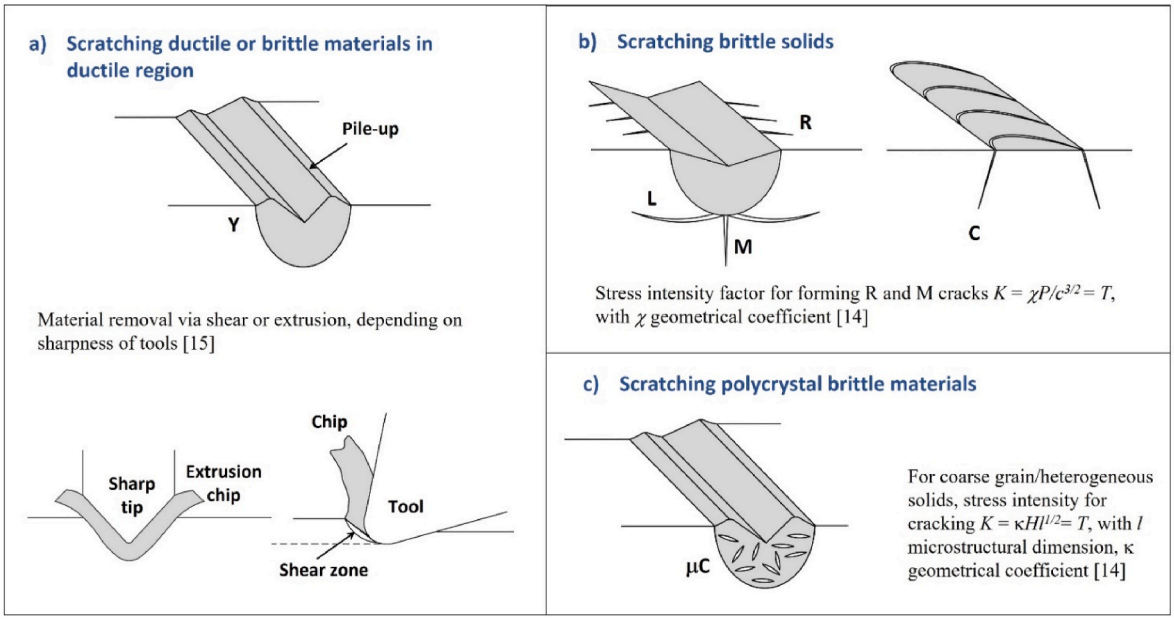

Fig. 5. Deformation and damage patterns induced by scratching in (a) ductile materials or brittle materials deformed in ductile region; (b) single crystal brittle materials; and (c) coarse grain polycrystal brittle materials.

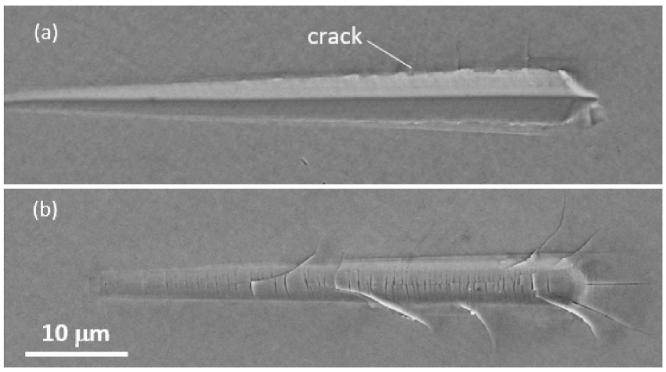

Fig. 6. Scratches of 50 mm long on GaAs single crystal substrate using (a) Berkovich indenter of tip radius of 200 nm and (b) conical indenter of tip radius of 5 µm, using a ramping load of 50 mN. *Note: these are the original research results from the authors' recent work and has not been published before.*

at 6 mN. The results shown in Figs. 6 and 7 provide several implications: *(i)* sharp indenters are in favour of promoting ductile removal; *(ii)* the value of d_c can be significantly affected by the indenter geometry (sharp or blunt); and *(iii)* cross-sectional TEM examination enables a complete characterisation of subsurface damage.

2.2. Scratching examples with off-the-shelf indenters

Scratching has been extensively used to mimic the deformation and removal events occurred in the precision machining of hard-to-machine materials, in particular brittle ones, as it can be performed in a precision instrument with controlled load and positioning. The method is simple, capable of testing samples at elevated temperatures with high strain rates. Post-mortem characterisation of the scratched surfaces can be carried out with ease using advanced materials analytical tools, such as SEM, TEM and Atomic Force Microscope (AFM) etc. Using this method, the relationship between mechanical load and removal mode can be understood, thus providing valuable knowledge for designing efficient machining processes. This is specially useful when dealing with new or unknown workpiece materials. In this section showcases how scratching can be done for this purpose are presented.

A review of the published literature revealed that there are almost no in-depth scratch studies on ductile materials (e.g. metals) strictly aiming to emulate and/or to provide deeper understanding of cutting mechanism. This is, somehow, not surprising since there are no significant changes in material response in deformation modes (i.e. ductile removal accompanied with lateral pile of material) when performing such tests.

However, more interesting aspects can be found when scratching hard and brittle single crystals, which can respond like ductile materials such as metals and alloys if the machining conditions are judiciously selected. Their damage patterns of the sublayer in ductile region include dislocations, stacking faults, slip lines, amorphization, formation of nanocrystals, lattice bending and distortion, etc [29]. Fig. 8 shows the cross-sectional images of silicon (Si) [30], gallium arsenide (GaAs) [22], and yttrium aluminium garnet (YAG) single crystals after scratching in the ductile region, whose damaged sublayers are dominated by dislocations, twinning, and slip lines, respectively. Careful analysis of Fig. 8 (a) indicates that an amorphous layer of silicon is on top of the dislocation layer, appearing in shallow grey colour. Amorphous silicon phase is easier to be removed than pristine Si via scratching [31], indicating that amorphization induced by mechanical loading in Si can benefit its removal in machining. This is supported by a great deal of machining studies on Si, which demonstrate that silicon is relatively easy to be machined in comparison to other brittle single crystals [32]. The composition and microstructure of a single crystal are expected to play a significant role in its deformation pattern under mechanical loading and hence the removal in mechanical machining [33,34].

In the subthreshold region of sliding contact, both the depth and density of crystallographic defects in the deformed subsurface increase with the enhanced loading. The depths of damaged sublayers in Si and GaAs caused by scratching were measured from TEM examinations [27, 30], and are plotted as a function of contact pressure in Fig. 9. Fig. 9(a) shows that scratching causes deeper damage in GaAs than in Si, while Fig. 9(b) demonstrates that a sharper tip generates less damage than a blunter one.

Soft-brittle single crystals are a unique class of brittle materials. Typical soft-brittle solids include potassium dihydrogen phosphate

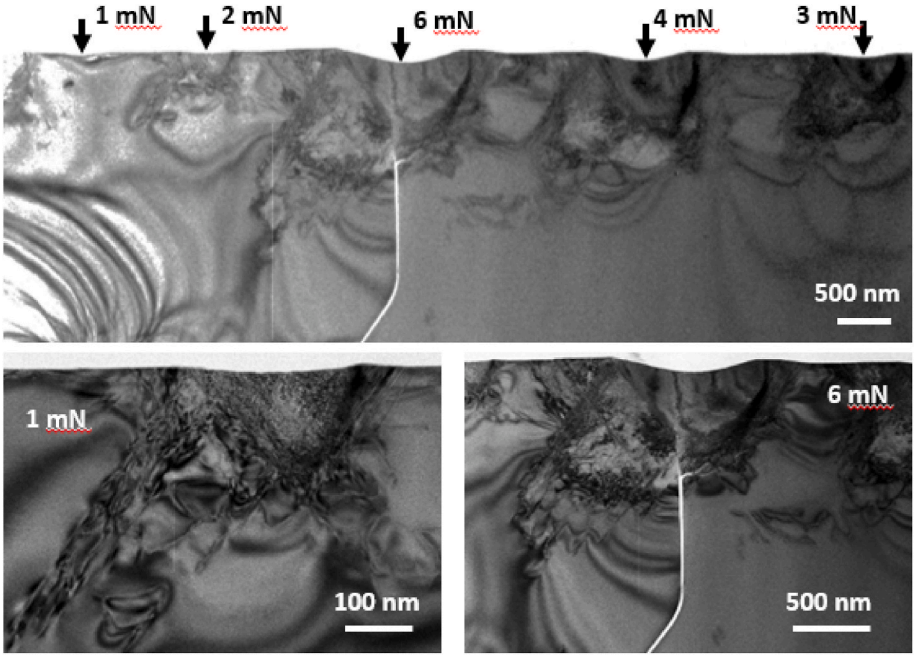

Fig. 7. Scratch on GaAs single crystal substrate using a conical indenter of tip radius of 3 µm and constant loads of 1, 2, 3, 4 and 6 mN. A median crack can be found in the sublayer generated at the applied normal load of 6 mN. Below 6 mN, the subsurface damage of the scratches is dominated by twinning [28].

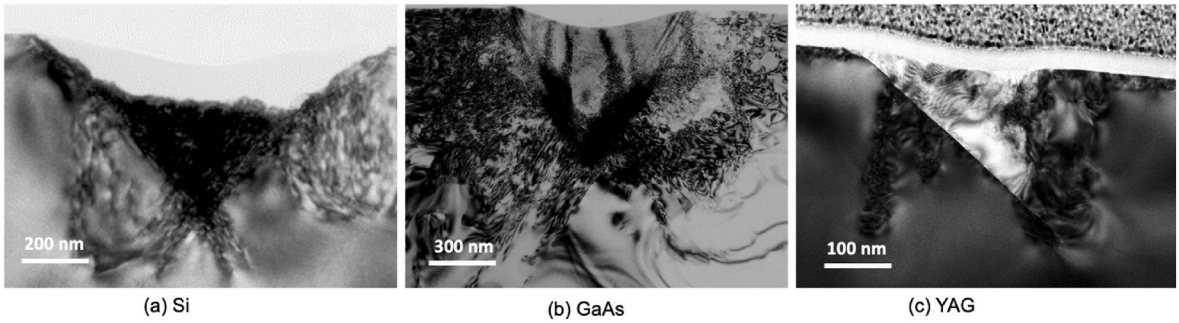

Fig. 8. Subsurface damage patterns of the scratches made on (a) Si [30], (b) GaAs [22], and (c) YAG single crystals using a conical indenter of tip radius of 3 mm in the subthreshold damage modes, where cracks are suppressed or contained.

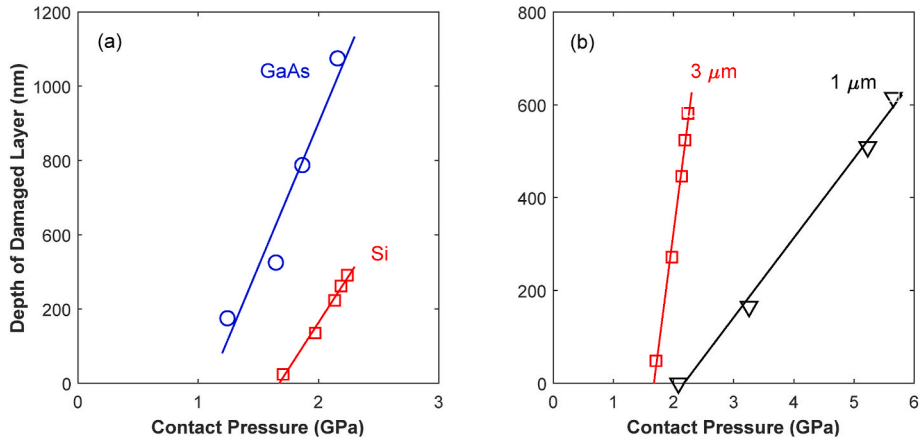

Fig. 9. Depths of the damaged crystalline sublayer measured from TEM are plotted as a function of the average pressure: (a) GaAs and Si scratched using 3 mm conical indenter, and (b) Si scratched using 1 and 3 μm conical indenters (data are collected from Ref. [28]).

(KDP), cadmium zinc telluride (CZT), mercury cadmium telluride (HgCdTe), zinc sulfide (ZnS), and calcium fluoride (CaF_2). They are highly important in a wide range of applications [35], such as radiation detectors, infrared detectors, optoelectronics and photonics devices, laser optics and solar cells. This class of materials have a quite low hardness (soft) but exhibit significantly high fragility (brittle). The peculiar property combination of 'soft and brittle' poses great challenges for fabrication, handling and machining, as damage is easily formed in their surface and sublayer during processing [36–40]. Cost-competitive processes for machining high quality substrates of such 'soft-brittle' materials are highly demanded. The key issue for the development is how to minimize surface and subsurface damages generated by mechanical removal while maintaining the required machining efficiency. In contrast to hard-brittle materials, many fundamental and important questions remain unanswered for soft-brittle materials. For instance, how are cracks initiated? How to characterise subsurface damage? How to determine the critical load for ductile removal? Comprehensive understanding of the deformation and fracture mechanisms of soft-brittle crystals involved in mechanical removal appears at infancy stage, and most of the previous developments of machining technologies still relies on approaches of trial-and-error. The characterisation of sublayer damage also lacks comprehension, likely because sample preparation for TEM is much more challenging than for hard-brittle materials.

The literature on the deformation and removal of soft-brittle materials are largely concerned with KDP crystals [41–44]. KDP is an important nonlinear optical crystal material, widely used in large-aperture high-power laser systems. Numerical and experimental scratching studies show that significant anisotropy exists in the material removal of KDP during scratching [43–45] and the integration of ultrasonic vibration [43] or heating [42] into scratching can promote ductile removal. Fig. 10(a) shows the TEM subsurface damage of a scratched CTZ single crystal, where stacking faults and some twins and dislocations are seen. The occurrence of stacking faults in CZT was accompanied with the formation of partial dislocations and twins [46]. Nanocrystals were also found in the scratch-induced deformation in CZT, near the top surface, as shown in Fig. 10(b). In contrast to the well-known hard-brittle materials, such as Si or GaAs, CZT has a relatively low density of crystallographic defects in the sublayer generated by scratching. In this study [46], the TEM specimens were carefully prepared by cutting and grinding, followed by ion beam thinning using a precision ion polisher and electron beam was parallel to the scratching direction to avoid any possible damage. Characterisation of the sublayer damage of soft-brittle materials apparently needs more research efforts [47].

Scratching at micro/nanoscales has found many successful applications in the understanding of deformation and removal mechanism of various polycrystal ceramics [48–52]. In this class of brittle materials, the effect of material microstructure is apparent and significant. Single grit-scratching of alumina [52] showed that for fine grain composition it has greater critical depth for ductile-to-brittle transition than the coarse grain one, as displayed in Fig. 11, where the 2 μm grain alumina can have a cutting depth of 6.1 μm before damage was found around the scratch, in comparison to the 3.7 μm for the 25 μm grain alumina. Surface fragmentation appears the major removal mode in the brittle region of both coarse- and fine-grained alumina.

A cross-sectional surface analyses of the scratched alumina [53] demonstrated that sublayer damage patterns are significantly different for coarse- and fine-grained alumina ceramics. As shown in Fig. 12(a), the material removal for the 3 μm grain alumina was mainly removed in the ductile region, and scratching induced both lateral and median

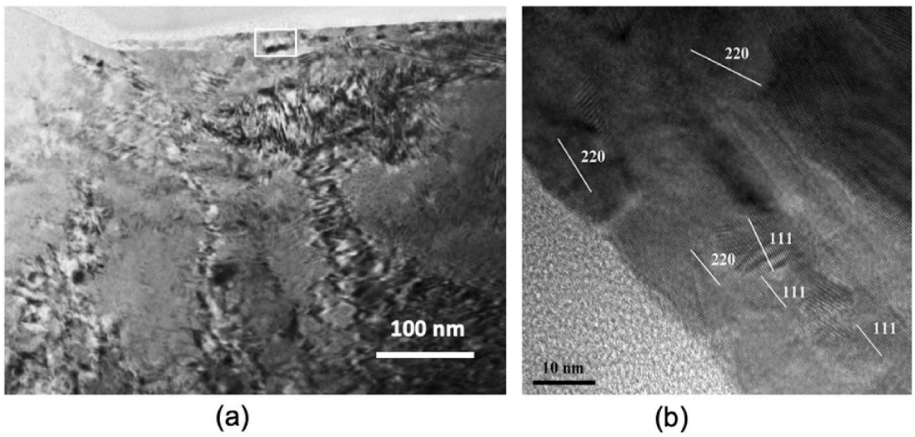

Fig. 10. TEM images of subsurface damage of a CTZ single crystal scratched using a Berkovich tip with a tip radius of 100 nm at load of 1 mN [28]: (a) low magnification view and (b) enlarged view acquired from the white rectangle in (a).

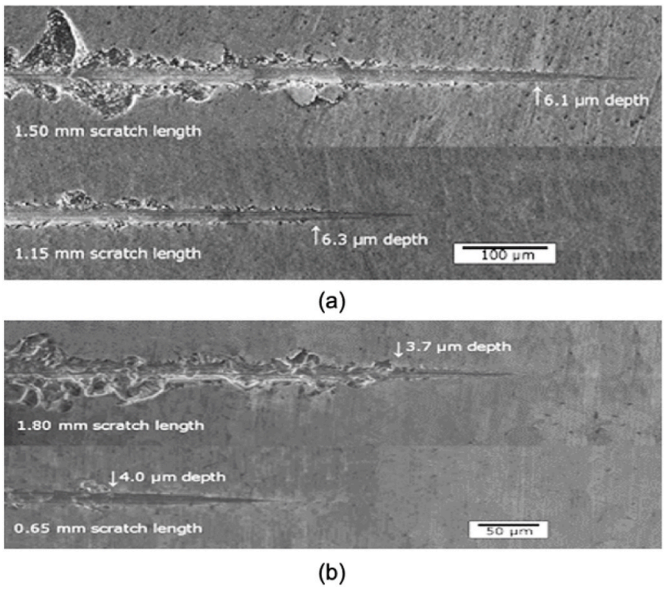

Fig. 11. Ramp load scratching of alumina ceramics with a 90-degree included angle phono-point diamond dressing tool of a tip radius of 5 μm: (a) 2 μm and (b) 25 μm grain size [52].

cracks in the sublayer, while in the sublayer of the 35 μm grain alumina the damage includes zigzag microcracks along the grain boundaries with presence of twin/slip bands as displayed in Fig. 12(b). The long-crack toughness values of the coarse and fine alumina are 3 and 4.8 MPa $m^{1/2}$, respectively, suggesting that the coarse-grained microstructure is more tolerant to long cracks. In general, the results shown in Figs. 8 and 9 indicate that fine-grained ceramics has better machinability than the coarse-grained one in terms of ductile removal, which is supported by a great deal of previous grinding studies [e.g. Ref. [54]]. In the scratching of polycrystal ceramics, scratching load, speed, and pattern [53], as well testing environment [55] can affect the critical load for initiation of several cracking, as well as fracture mode.

Glasses play an integral role in the manufacturing of modern products, with diverse uses in electronics, photonics and optics devices, energy and environmental components, and consumer appliances. Scratching of soda-lime glass shows a clear transition of deformation from brittle to ductile region when the indenter is sufficiently sharp and normal load is small enough [56]. At a relatively small load in scratching, glass was removed in ductile region with formation of apparent ductile chips and without generation of brittle fracture or cracking; while at a greater load, scratching induced cracks [57]. Introduction of ultrasonic vibration into scratching can improve glass machinability. In other words, the critical load or cutting depth for ductile removal can be increased if scratching is carried out with the assistance of ultrasonic vibration. Fig. 13 displays the groove formed on a glass surface via ultrasonic vibration cutting, clearly showing that the removal of glass transits from ductile to brittle mode when the depth of cut exceeds a threshold [58]. Increased scratching speed has apparent effect on the removal pattern of glass, generally promoting the removal towards ductile region [59,60].

2.3. Micro-cutting with edges that replicate real cutting tools

As mentioned in Section 2.2, in most (micro)scratch studies, standard indenters (e.g. Berkovich, Vickers, conical) are used as scratching

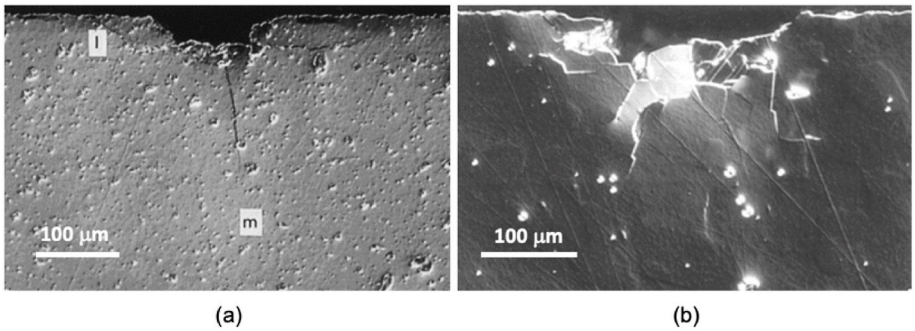

Fig. 12. Subsurface damage of alumina ceramics of (a) 3 μm and (b) 35 μm grain size after repeated scratching using a conical indenter with an apex angle of 120° and a tip radius of 10 μm [53].

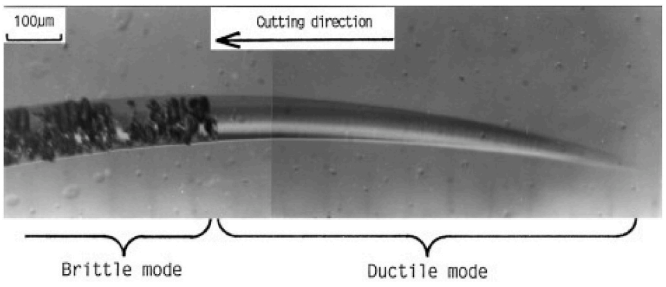

Fig. 13. The groove formed on a glass surface using single grit cutting with assistance of ultrasonic vibration, where a clear transition of brittle to ductile can be seen [58].

tools. This is acceptable when simulating grinding. However, if such indenters are used to simulate cutting in which the tool has well-defined rake/flank faces and specific rake/relief angles, the nanoscratching results will be inconsistent with the cutting results. To overcome this problem, many attempts have been made using carefully prepared cutting edges (with geometries similar to real cutting tools) for the fundamental investigation of cutting mechanisms at micro/nano scale.

A typical example is the plunge-cutting test that is, here, exemplified for single-crystal silicon [61] test piece on an ultraprecision machine tool which enables nano-to micro-scale precise change of depth of cut. Since silicon is an anisotropic material, several microgrooves in different directions are cut, as illustrated in Fig. 14(a), to investigate the influence of crystal orientation on the critical depth of cut. Fig. 14(b) shows the microscope images of microgrooves cut along different directions. From right to left, as the depth of cut increases, the microgrooves gradually broadened, and microcracks begin to form when the depth of cut reaches to a certain value, i.e., the critical depth of cut. When the depth of cut continues to increase, the density of the microcracks increases. Therefore, a clear ductile-to-brittle transition boundary can be identified on the groove surface. It is obvious that the critical depth of cut of silicon varies in different cutting direction, indicating that for crystal materials the quality of machined surface will be influenced by cutting directions. Moreover, by changing the rake angle of tool in microgroove plunge-cut test, the effect of tool rake angle on critical depth of cut can be presented in the same way. Fig. 14(c) shows the change in the critical depth of the cut as a function of cutting direction and tool rake angle. The results indicate that a moderately negative rake −30° angle is helpful for obtaining a ductile-cut surface. Among the three cutting directions, the 22.5° direction has the highest ductile machinability. The variation in the thickness of subsurface amorphous silicon layer with depth of cut for different cutting directions are observed by X-TEM, as shown in Fig. 14 (d). For each cutting direction, the amorphous layer thickness increases gradually with the depth of cut. As a general trend, the amorphous layer is thickest in the 45° direction and thinnest in the 22.5° direction.

As another example, a single-crystal diamond cutting tool with a straight cutting edge was used on an ultraprecision diamond turning machine to cut micro grooves on polycrystalline copper to investigate the formation of surface step at grain boundaries, and the results were compared with 2D crystal plasticity finite element simulations. The effects of both extrinsic cutting edge radius of diamond cutting tool and intrinsic misorientation angle of grain boundary on the propensity of grain boundary surface step formation were also examined [62].

Instead of using an ultraprecision machine tool, such microgroove cutting can also be performed using a versatile nanoscratching system and customized diamond indenters, with similar geometries of the real cutting tools, to perform nano-cutting tests [36,63]. Fig. 15(a) shows a typical cutting tool-like indenter, which has a −45° rake angle, 29° relief angle, 5 mm nose radius, and 115 nm edge radius. After the scratching by using this indenter, the formed microgroove and chip have a similar shape to those produced by real cutting tool, as shown in Fig. 15(b).

While both the ultraprecision machine tool and versatile nanoscratching system can only be employed in ex-situ microscope condition, the material removal and chip formation processes cannot be precisely investigated. Hence, to further explore the machining mechanisms of nanoscale cutting, developing a micro/nano-cutting unit integrated into the SEM is a promising technique for in-situ observation of surface and chips formation, which also facilitates the verification of simulation results [64]. This allows the in-situ investigation of the deformation on the sample surface plane; on the other hand, it is possible to consider the

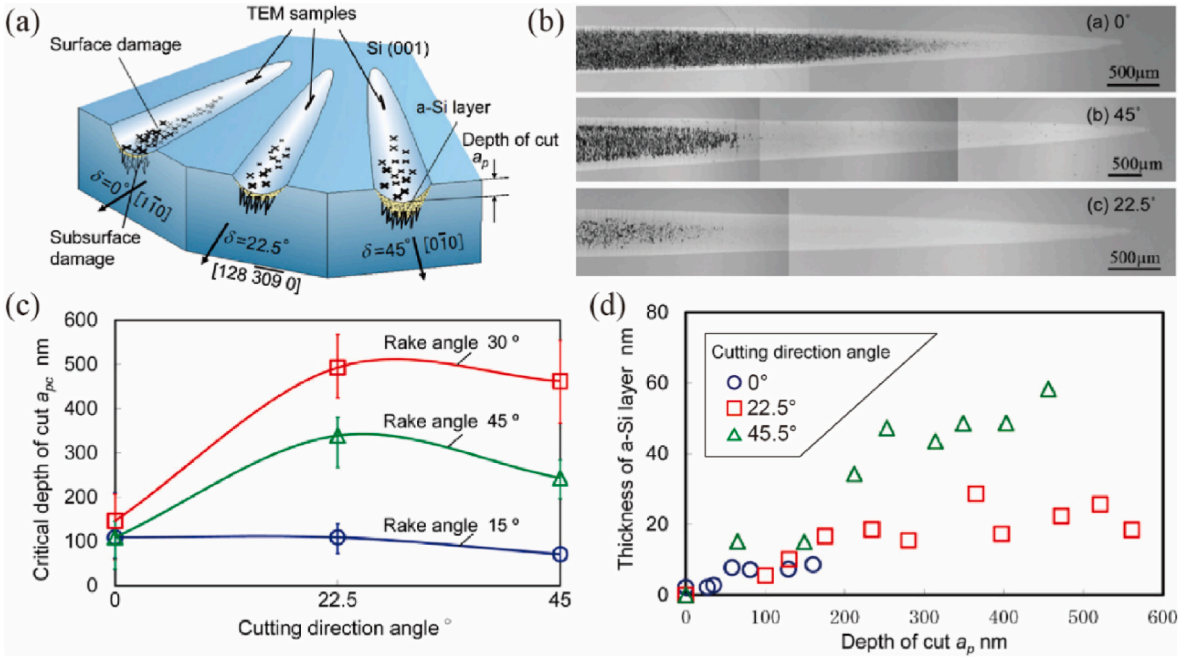

Fig. 14. Plunge-cut microgrooves on single-crystal silicon in different directions: (a) Schematic of experiment, (b) micrographs of microgrooves, (c) summary for the critical depth of cut, and (d) summary for the thickness of subsurface amorphous silicon layer [61]. (For interpretation of the references to colour in this figure legend, the reader is referred to the Web version of this article.)

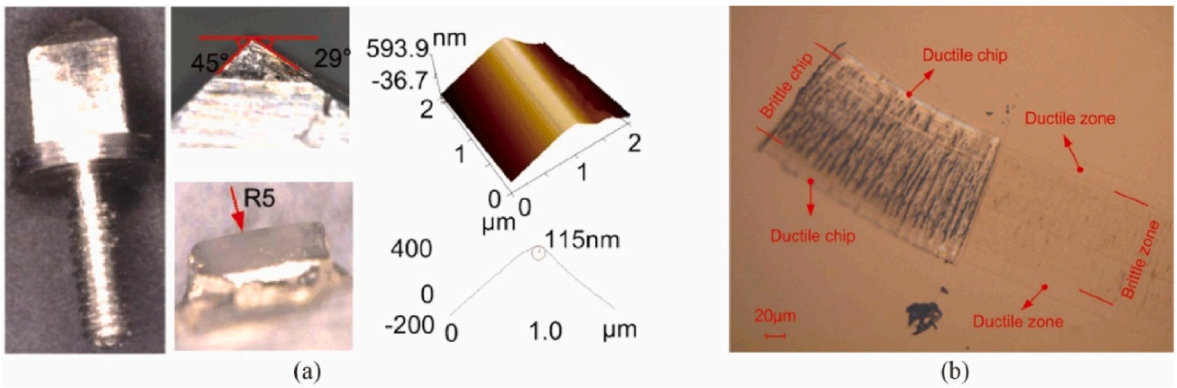

Fig. 15. Microgrooving by using general nanoscratching system equipped with a real cutter-shaped indenter: (a) geometry of the indenter, and (b) morphology of the microgroove by the indenter [36].

deformation of individual grains. Ueda et al. pioneered micro cutting of metals in an SEM for real-time observation of changes in shear angle and chip morphology with workpiece crystal orientations in 1980 [65]. A nanometric cutting device under high vacuum conditions in a scanning electron microscope was developed which could realize a displacement of 7 μm. Using a diamond cutting tool formed by focused ion beam (FIB) processing, nanometric cutting experiments on single crystalline silicon were performed under SEM online observation. Cutting depths of less than 10 nm could be obtained with high repeatability. Taper cutting and sinusoidal cutting were performed to study the material removal behaviour.

Another recent example is in-situ SEM micro-cutting on polycrystalline Nickel based superalloy [66], as shown in Fig. 16. A customized diamond (electrically conductive) cutting tip with well-defined geometry (rake angle: 0°; clearance angle: 30°; tip width: 10 μm; and tip radius: 90 ± 5 nm) is employed for the micro-cutting tests, as shown in Fig. 16(a) and (b). The cutting chips generated during the single grain and cross-boundary nano-cutting is captured by SEM, as shown in Fig. 16(c) and (d), hence, to investigate the chip and surface formation mechanisms. It can be clearly seen that the thicknesses of the chip produced in cutting grains A and B are different; the grain boundary (indicated by the dashed red line) is the dividing line of

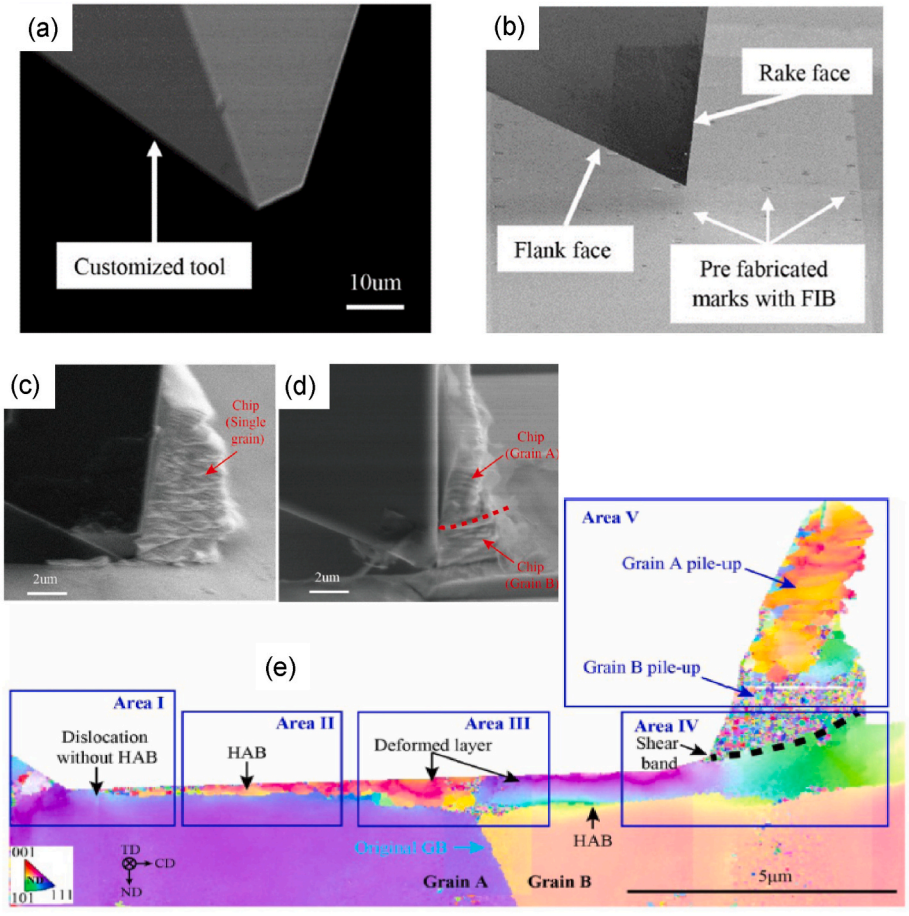

Fig. 16. In-situ SEM micro-cutting test on polycrystalline Nickel based superalloy: (a) and (b) image of diamond micro-cutting tool (90 nm edge radius), (c) and (d) image of chip morphology when nano-cutting in a single grain and across a grain boundary, and (d) full TKD map upon micro-cutting across a grain boundary [66].

chip morphologies. Followed by a full transmission Kikuchi diffraction (TKD) mapping on the cross-section of the machined surface and the generated chip, a significant variation in crystal orientation within the deformed layers of both grains A and B in comparison with substrate material is observed, which confirms that the initial crystal orientations indeed affect the surface integrity of grains for a same nano-cutting condition.

A more ductile material, aluminium 7475, was also examined by the in-situ SEM micro-cutting method to reveal the size effect on the cutting energy at machining process [67]. The observation of chip formation indicates the material deformation is concentrated in a narrow region around a shear line and reveals the development mechanism of primary shear zone under micro scale, as shown in Fig. 17. A cutting forces measurement setup at deep submicron feeds and cutting tool apex radii was also developed which enables the discrimination of different sources for the size effect on the cutting energy. Through this test, it proves that typical industrial values of feed and tool radius imposes a size effect determined primarily by geometrical factors, while in a sub-micrometre feed range the contribution of the strain hardening in the primary share zone becomes relevant [67].

However, while most in-situ SEM micromechanical testing system are designed for a relatively low speed test due to the setup scale limitation, by employing these off-the-shelf systems to replicate the cutting process the cutting speed/strain rate is limited compared to a real cutting condition. Hence, to enable an ideal platform for the installation of largescale in-situ SEM cutting (i.e. turning) experiments, a large-chamber SEM has been developed as shown in Fig. 18 [68]. In this development, exploiting the large space in the sample chamber, SEM column can move around the sample and image it from freely selectable viewing directions, due to an integrated with positioning system (Fig. 18 (b)). A special turning setup has been developed, including two linear axes which are arranged orthogonally to one another and a workpiece driven in rotation (Fig. 18(c)). This allows the higher speed cutting compared to the off-the-shelf in-situ SEM micromechanical testing system. For this case, a metallic sample can be turned with a precision in the range of a few μm and velocities up to 100 μm/s. The resulting turn track, the deformation on the surface, and the resulting chip were examined in-situ with this large chamber SEM setup. Eventually, the chip formation on the microstructure scale can be observed during the machining process while the fundamentals for the understanding of the mechanisms which cause modifications of the surface near zone during straining of the material have also been revealed, as shown in Fig. 18(d) and (e).

2.4. Limitations and challenges of scratch-like tests with off-the-shelf/customised tips

While scratch-like tests with common/customised tips are capable to elucidate some effects of mechanical load on the material deformation and removal at microscale or even nanoscale, they are not able to completely mimic the conditions involved in a real cutting or abrasive processes. Typically, scratching at micro or nanoscale cannot reach the cutting speed that is used in machining; thus, the effect of strain rate on the material deformation is not included. Such knowledge could be particularly important for the materials whose deformation is sensitive to strain rate. In an abrasive machining process, a workpiece material experiences repeated scratching at the same location and multiple scratches are made at the same time, and the induced heat and its dispassion is different from single scratching test. A much higher temperature would be induced in the machining, causing different thermal effects. Scratching often uses off-the-shelf indenters that have conical shapes at tip. Thus, their tool geometries are also different. When designing a machining process using the knowledge gained from scratching, these effects must be considered.

2.4.1. Effect of strain rate

The cutting speed used in abrasive machining or diamond cutting is at the scale of m/s, while that for instrumented scratching is several orders lower, usually at mm/s and sometimes much smaller, e.g., even at microns/s. The strain rates associated with the deformation of a work material are considerably different. In high-speed machining strain rates can be further increased by several orders of magnitude than conventional one. The mechanical load induced deformation in many metals and alloys is strain rate sensitive [69–71]. Some of brittle materials are also sensitive to the change in strain rate [72–74]. Therefore, to design an optimal machining process, particularly for determining the critical depth of cut for ductile removal in a brittle solid as defined in Eq. (5), the strain rate effect must be considered.

For example, in the high-speed scratching of BK7 glass [60], the lateral cracks generated at 20 m/s are in a shallower sublayer than those induced at lower speeds of 1 and 5 m/s 'Micro-shear' observed at the speeds of above 5 m/s occurred earlier when the scratching speed was increased, which might be attributed to the less damage caused at higher speeds. The outcomes are supported by the so-called 'skin effect' observed in some previous machining studies [75]. On the contrary, in the single grit cutting of gallium oxide that used scratching speeds varied from 13 to 67 m/s [76], a higher speed generated longer median cracks. The effect of strain rate appears microstructure related.

A high strain scratching or cutting speed leads to an enhanced adiabatic heating at the microcontact sites [77], which should increase the temperature in the contact zone of abrasive machining or diamond cutting. The temperature increase reduces the tendency of cracking, thus promoting ductile removal. The details on the role of temperature in material removal will be discussed in the later section in this review.

To close this gap due to strain rate, from the aspect of material property, the strain rate-insensitive materials, such as Ni-based super alloys [78], may be selected to investigate the effect of other factors on the machining mechanisms. From the aspect of numerical analysis,

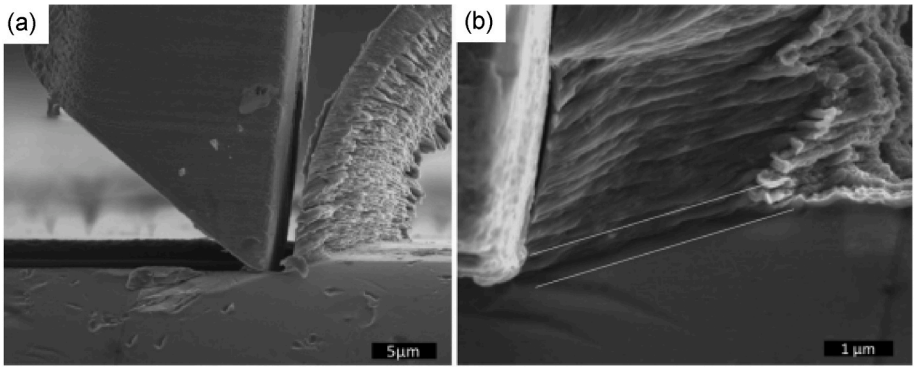

Fig. 17. In-situ SEM micro-cutting test on aluminium 7475 (a) Lateral overview of the system workpiece-chip-tool. (b) Steady state shape of fully developed PSZ [67].

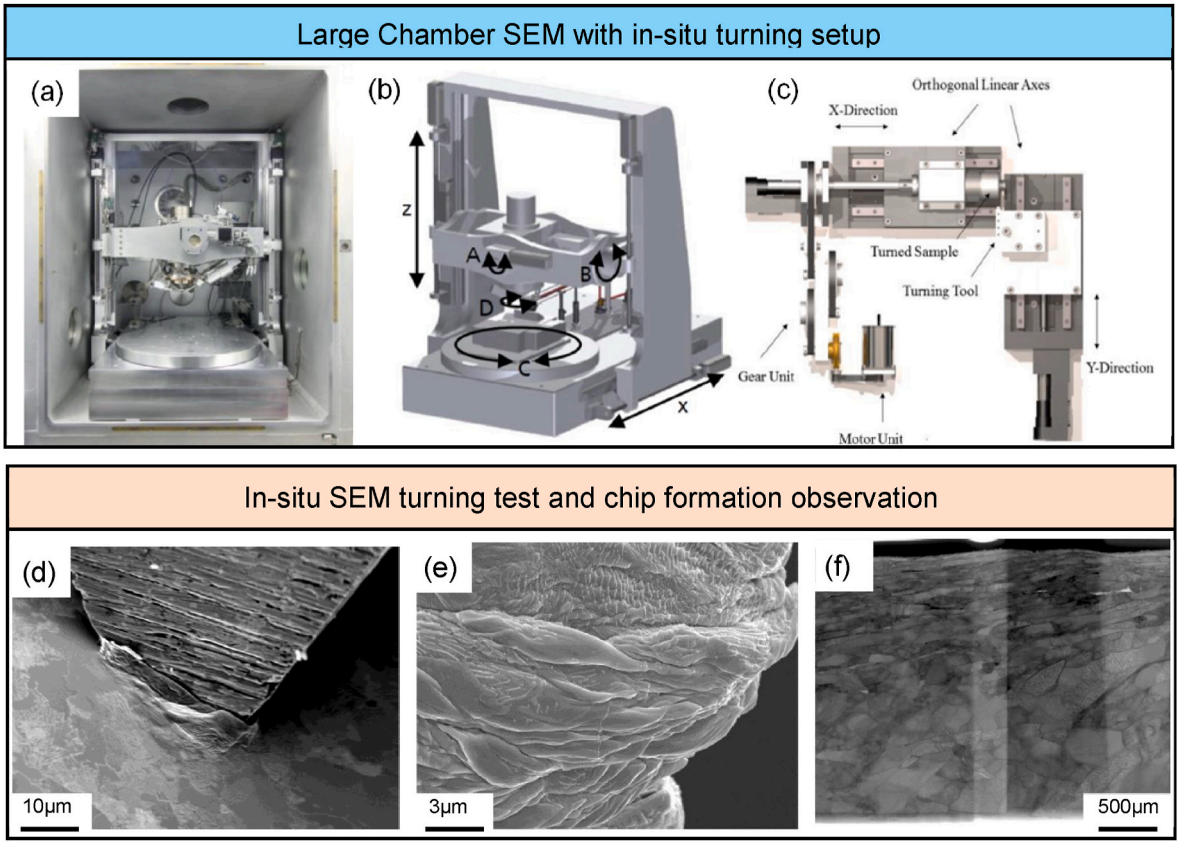

Fig. 18. (a) Large chamber for SEM with an inner dimensions: 1,2 m (w) x 1,3 m (h) x 1,4 m (d); (b) Schematic drawing of the positioning system; (c) In-situ SEM turning device; (d) In situ cutting experiment; (e) Magnification of a chip; (f) TEM observation of the machined surface [68].

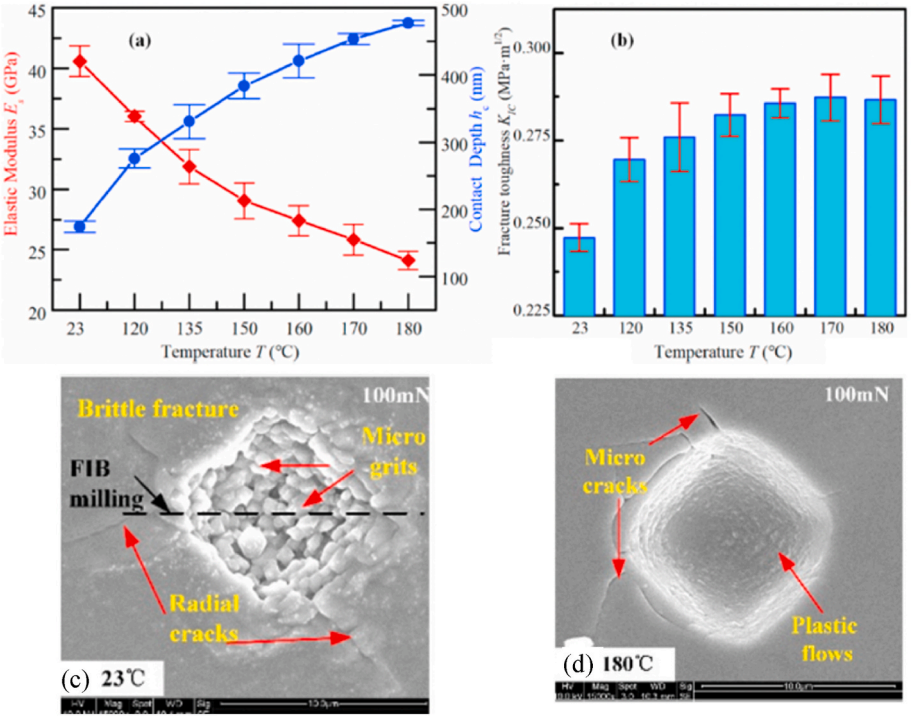

Fig. 19. (a) The elastic modulus and contact depth and (b) fracture toughness at different temperatures; indentation impressions reveals (c) brittle fracture at room temperature and (d) plastic flow at high temperature indentations [42].

developing strain rate-dependent constitutive models will be an effective approach to simulate the machining mechanism of strain rate-sensitive materials. From the processing aspect, high strain rate machining setups, such as turning in SEM [68], have been developed recently.

2.4.2. *Effect of temperature*

Temperature can significantly influence the materials mechanical properties and eventually influence the chip formation mechanism, e.g., the brittle-to-ductile transition of brittle materials. In the real machining, e.g., turning, drilling and grinding, the material removal is a continuous process whereby the cutting energy/heat can be easily built up under high cutting speed, in which conditions the materials can undergo a softening regime when compared to the room temperature. An example of KDP crystal (a soft-brittle material) is shown in Fig. 19, whereby a decreased hardness and elastic modulus as well as increased fracture toughness have been observed with the increase of temperature, indicating that a higher capacity of plastic deformation at elevated temperature may occur in machining [42]. However, in conventional micro and nano scratching/cutting test, where relatively slow cutting speeds are employed, the temperature effect cannot be observed.

Hence, to observe the temperature effect in the micro and nano scratching and cutting test, normally an external heating process can be added during the test. This requires the heating stage to be built with the testing jig whereby the temperature of the test piece can be controlled precisely. In this scenario, micro scratching test can clearly reveal the difference of the material removal mechanism under different temperatures at the micro-level. Fig. 20 shows an example on KDP scratching at different temperatures. At room temperature, brittle cutting mode dominates the scratching process with the increase of applied load, whereby parallel cracks, shell-shaped fractures, and micro grits take place while material is removed mainly by severe edge chippings [42]. In contrast to the almost totally brittle scratch at room temperature caused by crack propagation and edge chipping, the scratch at 170 °C can achieve more ductile-regime surfaces with a larger critical undeformed cutting depth, smoother and less fluctuating surface, as shown in Fig. 20(b), due to the increased plasticity at high temperature. This reveals that in scratching the temperature effect can enhance the threshold of critical uncut chip thickness of brittle-to-ductile transition and the specific cutting mechanism of brittle materials. Hence, while the temperature effect is normally not considered during the micro scratching test due to the limitations of the test jig, this effect cannot be ignored.

Rapid temperature change can be also caused by the cooling effect of a coolant/lubricant. For example, in the cutting of single-crystal CaF2 wafer, it is found that thermal fracturing occurs (see Fig. 21(a) B-region) when the tool feed rate is small and the lubricating oil is used, which makes ductile machining difficult to achieve [79]. This is because the cutting-induced heat causes the temperature of the near surface region to rise significantly compared to the interior material. The high surface temperature, however, drops rapidly due to the cooling effect when a cutting fluid is used. If the thermal conductivity of material is extremely low (thermal conductivity of CaF2 is 0.06 times that of silicon) and thermal expansion coefficient is extremely high (thermal expansion of CaF2 is 5.8 times that of silicon), a significant temperature gradient

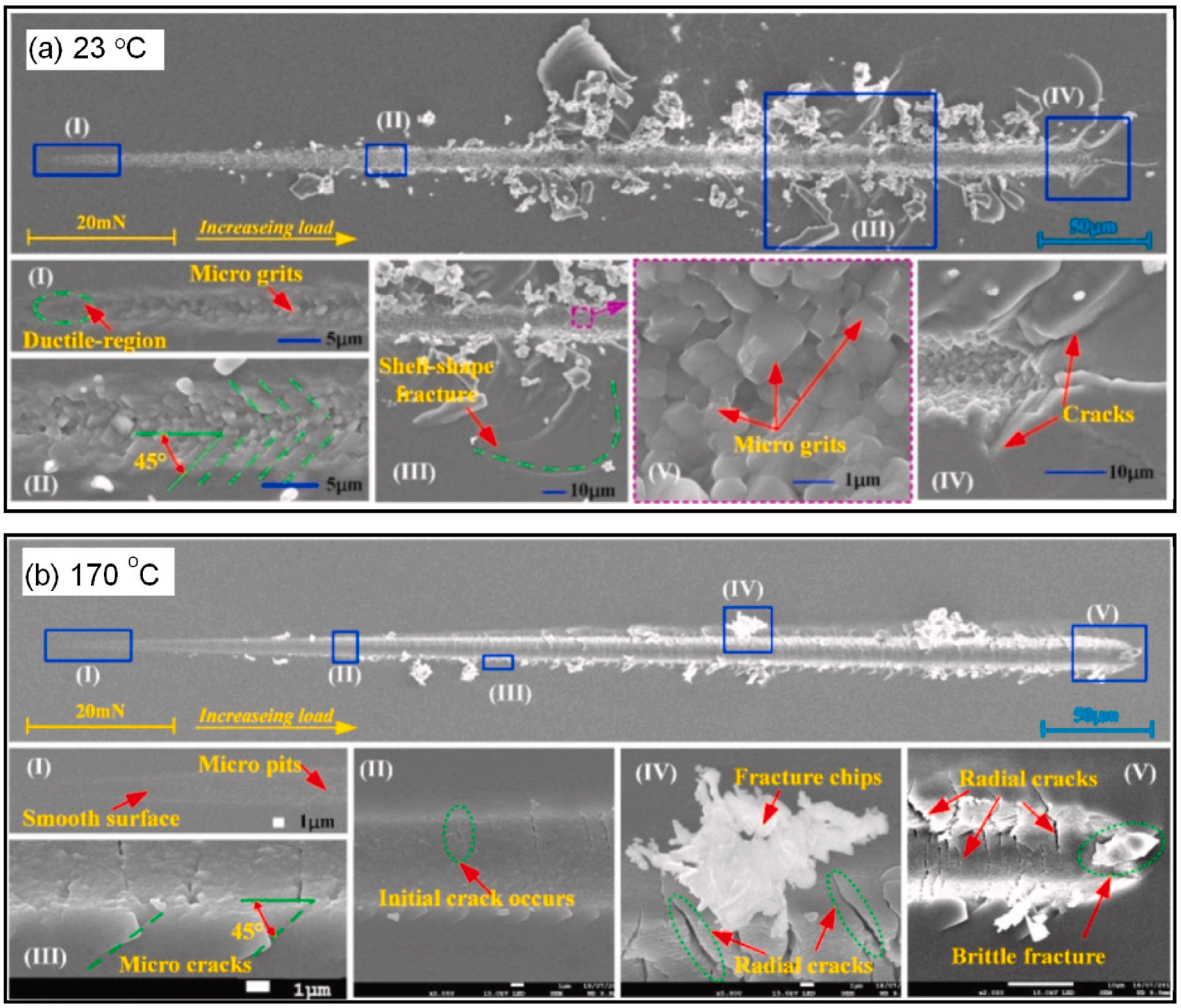

Fig. 20. The scratch surface morphologies processed at (a) room temperature and (b) elevated temperature [42].

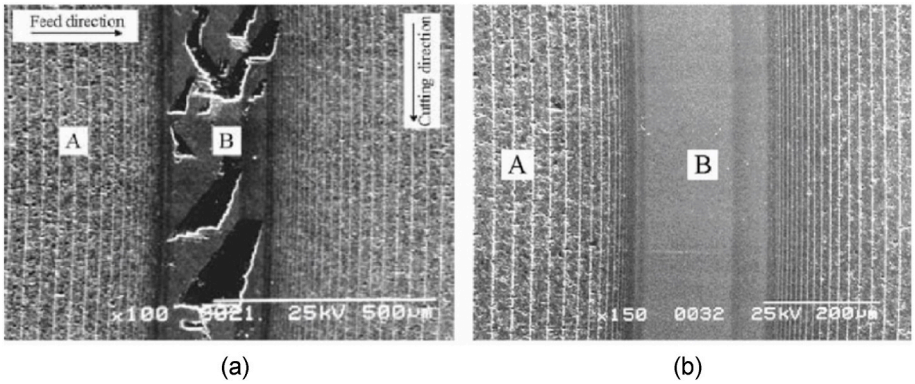

Fig. 21. SEM images of the CaF2 surfaces machined at continuously varied tool feed under (a) cooling condition, and (b) dry conditions [79].

results, consequently leading to a sharp stress gradient between the near surface layer and the internal region, which drives crack initiation. Furthermore, although high temperature nanoindentation and nano-scratching can be performed, the temperature gradient in the workpiece is much more uniform as heating system is integrated within the nanoindenter system, which is very different from the conditions occurring in real cutting.

2.4.3. *Effect of tool geometry/movement*

2.4.3.1. For scratching test. It is generally accepted that in grinding of materials with different mechanical properties, sharper grits with higher aspect ratios are effective in use against softer materials where cracking is less prevalent, but for harder materials some degree of bluntness is more appropriate to enhance ductile removal [24]. Therefore, when designing a machining process using the knowledge gained from scratch testing, effects of tool geometry must be considered. However, scratching often uses off-the-shelf indenters that have pyramidal and conical tips, as introduced in previous sections of this paper, making it difficult to exactly simulate the situation of a real grinding process where enormous grits of random sizes and shapes scratch the workpiece simultaneously. In nanoscratching tests, the contacts between the indenter and the workpiece are usually simplified to two cases, sharp contact and blunt contact, according to the indentation mechanics [23]. The stress field beneath a sharp contact is predominantly plastic or quasi-plastic, while that beneath a blunt contact is predominantly elastic [14].

Spherical and Berkovich-type indenters are two most commonly used off-the-shelf indenters in nanoscratching tests, which simulate the sharp contact and blunt contact, respectively. Fig. 22(a) and (b) show the examples of spherical and Berkovich-type indenters, which have tip radius of 10 µm and 40 nm, respectively. In addition, as the geometry of Berkovich-type indenter has flat faces and sharp edges (see Fig. 22(b), it allows to be set to face-forward (FF) or edge-forward (EF), as shown in Fig. 22(c). This is useful for simulating grinding with randomly shaped and distributed gits, especially diamond grits which have sharps tips, ridges and faces.

A typical example is shown in Fig. 23, demonstrating the effect of tool geometry on surface and subsurface formation in the nano-scratching of ZnSe poly crystal [80,81]. For the Berkovich-type indenter, when it scratches workpiece in the FF direction, periodical fishbone-like patterns are formed along the scratch path. Besides, the slip lines which are characterized by a number of fine straight lines parallel to each other are found in front of the indenter, and they are limited to the area within the indenter-workpiece contact width, as shown in Fig. 23(a). While when it scratches workpiece in the EF direction, the fishbone-like pattern has a direction opposite to the pattern formed in the FF direction, and the slip lines appear emanating from the edge of the groove, as shown in Fig. 23(b). This infers that shear deformation in front of the indenter is the predominant deformation behaviour in the scratch in the FF direction, whereas side flow of the material dominates the deformation behaviour during scratching in the EF direction. From the Raman mapping analysis, it can be seen that in the groove scratched in the FF direction (see Fig. 23(d)), the Transversal Optical (TO) peaks at the centre of the grooves moved to a lower Raman shift, indicating tensile residual stress in the subsurface of the scratched groove, whereas, in the groove scratched in the EF direction (see Fig. 23(e)), the TO peaks at the centre of the grooves moved to a higher Raman shift, indicating compressive residual stress in the subsurface of the scratched groove. For the spherical indenter, a smooth surface free of fishbone-like

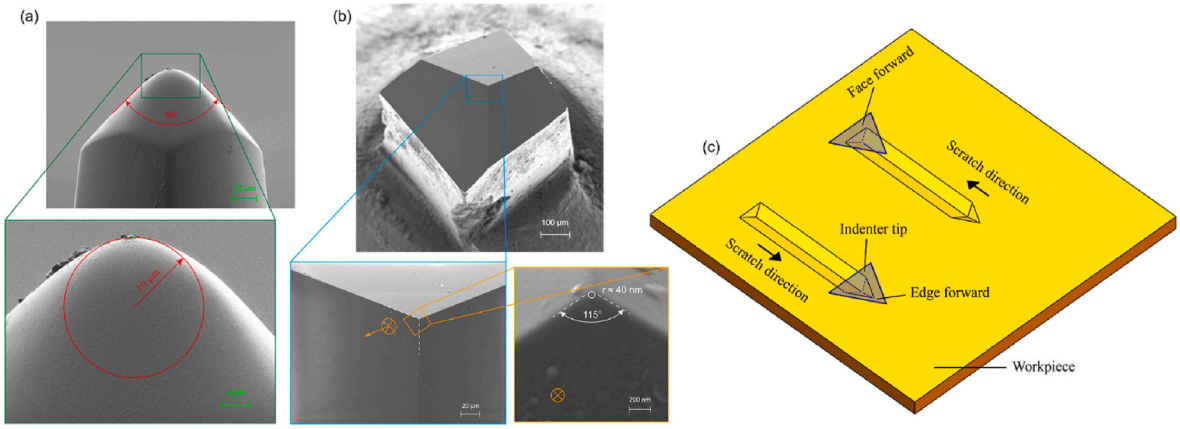

Fig. 22. SEM images of (a) a typical spherical indenter [80], and (b) a typical Berkovich indenter tip [81]. (c) Schematic of the nanoscratching process using Berkovich indenter to scratch workpiece in face-forward and edge-forward directions.

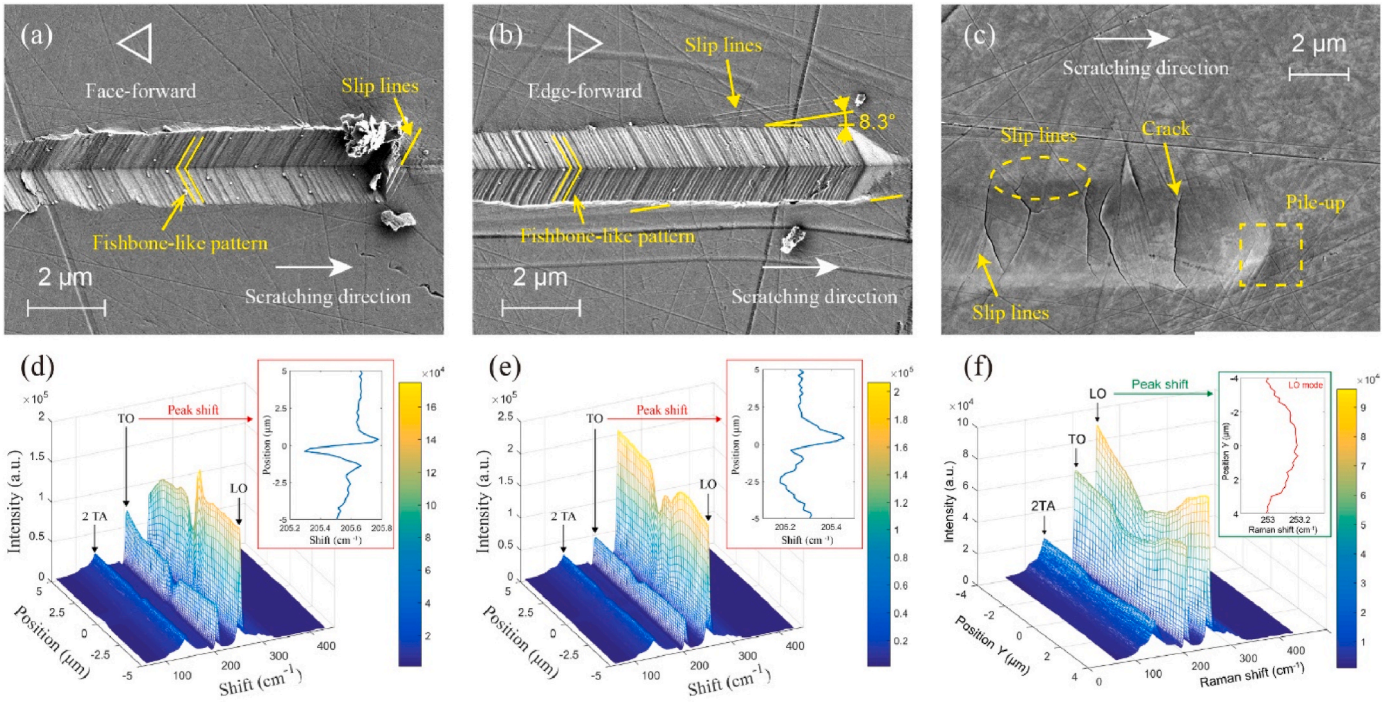

Fig. 23. SEM images of the grooves scratched on poly crystal ZnSe wafer by using (a) Berkovich indenter in face-forward direction, (b) Berkovich indenter in edge-forward direction, and (c) spherical indenter. (d)–(f) Raman mapping of the scratched grooves shown in (a)–(c) along the direction perpendicular to the scratching direction [80,81].

patterns is created, as shown in Fig. 23(c). Although many cracks form in the groove and pile-up forms in front of indenter, no material has been removed from the substrate, even though the normal load of scratching is much higher than when using Berkovich indenter. The Raman result presents that compressive residual stress is generated in the subsurface of the groove. These results indicate that when using a blunt indenter burnishing effect may occur.

Fig. 24(a) shows a microgroove machined on polycrystal ZnSe wafer, which is the same material as in Fig. 23, using a diamond tool. It can be seen, the surfaces of the groove are very smooth, though some cracks generate on the edges of the groove. More importantly, no pile-up forms next to the edges of the groove. Fig. 24(b) presents the diamond tool for machining the groove, which is featured by a flat rake face, sharp edge, and moderate rake/relief angles. It is known that in the machining process the tool rake angle, tool edge radius, and tool nose radius greatly affect the material removal behaviours. Therefore, due to the distinct difference in tool geometries between the off-the-shelf indenters and the diamond cutting tools, the material deformation behaviour in nano-scratching is likely very different from that in nano cutting. To better simulate the cutting process via nanoscratching, using customized indenters like real cutting tools is necessary, as introduced in Section 2.2.3.

Another limitation in scratching tests is tool feed movement. In most scratching studies, independent grooves generated by single scratches have been investigated without considering the tool feed movement, thus the interference and overlap among the neighbouring scratches could not be considered. However, in a real grinding process, and other abrasive machining processes, enormous grits of random sizes and shapes scratch the workpiece with significant interference and overlap. This leads to a gap to close for future research in this area.

2.4.3.2. For micro/nano-cutting test. As mentioned above, the commercial pyramidal and conical tips used for indentation test can be directly used for scratching test due to some similarities of their geometry of the undefined cutting edges, i.e., grinding grits. However, from micro/nano cutting point of view, to mimic the conventional cutting such as orthogonal cutting, turning and milling, the defined sharp cutting edges have to be applied to operate the material removal at micro/nano scale. In this sense, as the off-the-shelf indenters, e.g., Berkovich, spherical and

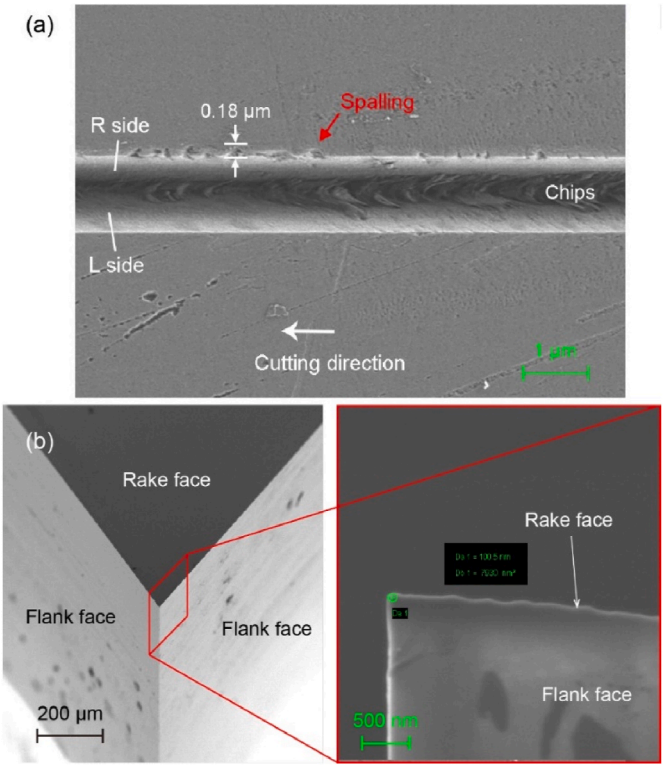

Fig. 24. SEM images of (a) a microgroove cut on a poly crystal ZnSe wafer, and (b) the diamond tool used for machining the microgroove [82].

cube corner tips, are normally designed for hardness test with pyramidal or conical geometries, none of them can be used for this purpose. Hence, in micro/nano-cutting scenario, the cutting tool is normally customized in diamond (electrically conductive) cutting tips with well-defined geometry for the nano-cutting tests.

In this circumstance, the cutting edge must be manufactured in a conscious way that enables the comparable dimensions for study the tool-crystal interaction, e.g., cutting within one grain or cross grain boundary. On the other hand, as the uncut chip thickness reaches a submicron/nano level, the tool edge should be sharp enough to eliminate the ploughing/size effect. That is, the tool edge radius must be smaller than 1/3 of the uncut chip thickness, as shown in Fig. 25, and make it normally under 100 nm [64]. Generally, the straight cutting edge could be applied with an edge length <10 μm while the rake and flank angles can be well defined through ultra-precision grinding or focused ion beam sharpening. Furthermore, cutting at this scale requires the workpiece to be strictly parallel to the cutting edge to make sure that the cutting depth of the machined surface is consistent [64]. For this, a T-axis stage is normally required to rotate the sample or tilt the tool at a certain angle.

In addition, like scratching studies, only independent grooves generated by single cuts have been investigated without considering the tool feed movement. However, in a real cutting process, such as turning and milling, the tool feed movement cause significant interference and overlap among multiple tool passes. This effect of interference and overlap among multiple tool passes is still difficult for the current in-situ micro/nano cutting setups.

2.4.4. Lubrication effect

To improve the machined surface quality and suppress the tool wear, lubricating media are widely used in cutting. For example, in the diamond turning of reaction bonded SiC, the lubricating oil mixed with different nanoparticles are applied to reduce tool wear [84] – see Fig. 26. Obviously, such studies on the effect of lubrication condition on tool wear cannot be carried out in nanoscratching test due to the extremely short scratching distance and, in some circumstances, because of the setup limitations (e.g. in-situ SEM is under vacuum). Nonetheless, the effect of lubrication condition on machined surface quality can be investigated to some extent by nanoscratching test. Fig. 27(a) and (b) show the grooves scratched on ZnSe poly crystal wafer under dry and lubricated conditions [80]. It can be seen that in dry condition the slip lines form both at the bottom and edge of the groove. At the end of the groove, a pile-up is observed, and the slip line emanates from the pile-up, which implies that as the tool moved forward, the pile-up in front of the tool is pushed aside, resulting in the formation of slip lines at the groove edge. In contrast, in the groove scratched under lubricated condition, the pile-up at the end of the groove is not evident; consequently, the formation of slip lines at the groove edge are less evident. It is believed that the lubricating oil helps to reduce the friction between the tool and workpiece, leading to a reduction of the material accumulation in front of the tool.

3. Micro-mechanical testing for studying the process outcomes

As presented in the overview in Fig. 3, the micro-mechanics instrumentations/methods not only can be used for emulating (with the above commented limitations) the cutting processes under control conditions but also for evaluation and in-depth characterisation of machine (sub) surfaces at micro/nano level, topic which is addressed in the following.

3.1. Nanoindentation for studying the mechanical property of machined surfaces

Nanoindentation is widely used for testing the mechanical properties of materials such as hardness, elastic modulus, and fracture toughness. It enables the use of different shaped (e.g. pyramidal, conical, and spherical) indenters and precisely controlled loads for deforming materials at submicron to nanometer level. There is a close relation between the deformation behaviour of material in nanoindentation and in micro/nano scale machining. For example, during diamond turning, as illustrated in Fig. 28(a), a damaged layer would form in the subsurface of workpiece as a strong machining pressure is produced beneath the tool. This is geometrically similar to the formation of subsurface damaged layer during nanoindentation, as shown in Fig. 28(b) and (c). Therefore, nanoindentation, especially in-situ nanoindentation in SEM [85] can be used to directly observe the surface fracture onset, crack propagation and delamination for brittle materials, pile-up, creep, elastic/plastic sink-in and shear band formation for metals, and time-sensitive phenomena for polymers, etc., which consequently assists understanding the machining processes.

Nanoindentation has been used to detect the mechanical properties of not only pristine bulk materials, but also workpiece surfaces after machining processes. Subsurface damage that occurs during machining is different for various materials. For example, the subsurface damage in steel/advanced alloys could be manifester usually a white layers and plastic deformations [87]; the subsurface damages from the cutting of high entropy alloys and ceramics are grain refinement [88,89]; the subsurface damages from the cutting of hard-brittle crystal (Si and Ga_2O_3) are amorphous phase layers and dislocations [61,90]; and the subsurface damages from the cutting of soft-brittle crystal (CaF_2, ZnSe, and HgCdTe) are dislocations only [36,91–93]. How the mechanical properties of these damaged layers have changed in comparison to the material before machining and how they affect the subsequent

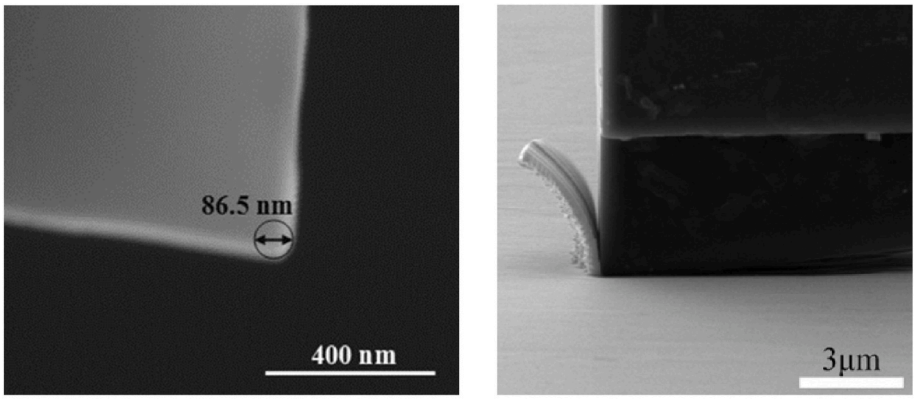

Fig. 25. SEM images of (a) customised tool edges and (b) tool-workpiece interaction in micro-cutting [64,83].

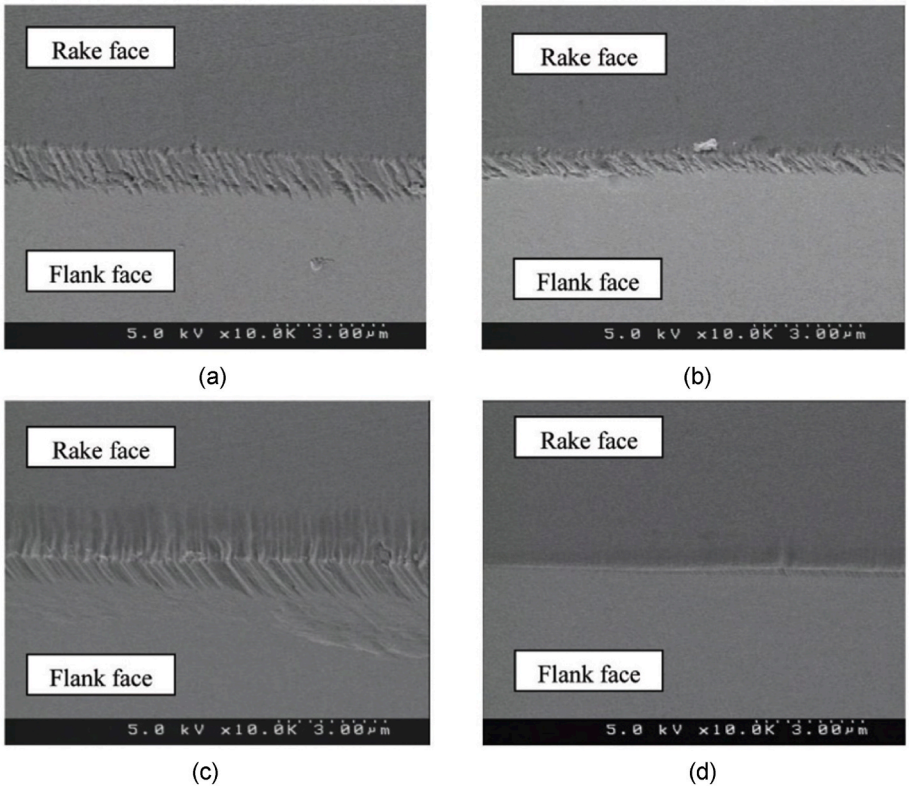

Fig. 26. SEM images of tool wear after machining reaction bonded SiC under the lubricating oil mixing with different nanoparticles: (a) MoS_2, (b) graphite fiber, (c) CuO, and (d) Cu [84].

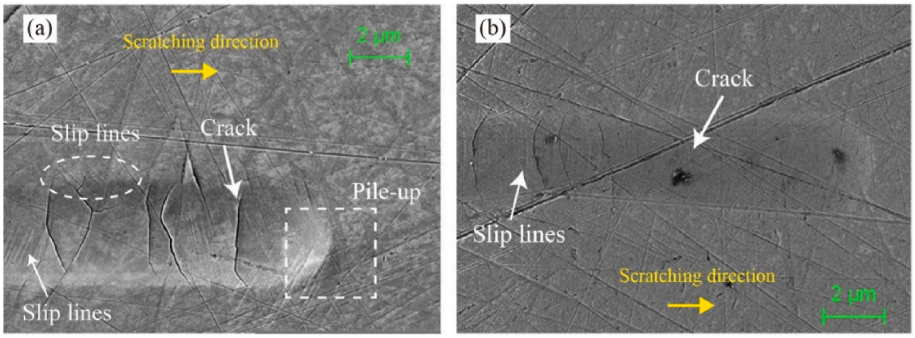

Fig. 27. SEM images of the grooves scratched on ZnSe poly crystal wafer under (a) dry condition, and (b) lubricated condition [80].

machining processes can be determined by analyzing the nano-indentation load-displacement curves of the material surfaces before and after machining. As such, this section mainly focuses on the use of nanoindentation tests for studying the mechanical properties (residual stress, hardness, elasticity, plasticity, fracture toughness, etc.) of the material surfaces after mechanical processing. The machining-induced mechanical property changes can be detected by analyzing the load-displacement curves of the nanoindentation and a series of post-mortem measurements (AFM, TEM, Raman spectroscopy, etc.).

3.1.1. Hardness and qualitative indications on residual stresses/material transformations

Two typical examples are shown here to demonstrate how to analyze the load-displacement curves of indentation for evaluating the residual stress and hardness of machined surfaces. Fig. 29(a) presents a cross-sectional image of a turned surface of AISI 52100 steel, displaying a subsurface damage layer, i.e., a white layer, with a thickness of over 50 µm [94]. Fig. 29(b) presents load-displacement curves for the indents performed on the sample cross-section with different distances from the machined surface [94]. At the near-surface region (~2 µm), the slope of the curve at initial yielding point (corresponding to indentation depth about 100 nm) is increased, indicating that residual stress in this region is compressive; while at the depth of 51 µm the slope of the curve at initial yielding point is decreased, indicating that residual stress is tensile or at least less compressive. However, it should be noted that the residual stress only affects the slope of load-displacement curve at onset of yielding, and the further plastic deformation induced by increasing the load could not give any information about residual stress. Also, it is not currently possible to measure residual stresses quantitatively by nanoindentation.

Fig. 30 presents load-displacement curves for nanoindentation tests on a chemo-mechanical polished silicon sample (pristine silicon) and diamond-turned silicon sample (machined silicon [95]. It can be seen that the maximum indentation load for both samples is 0.6 mN, but a larger displacement is obtained when performing indentation on the machined silicon. This indicates the hardness of the machined surface is

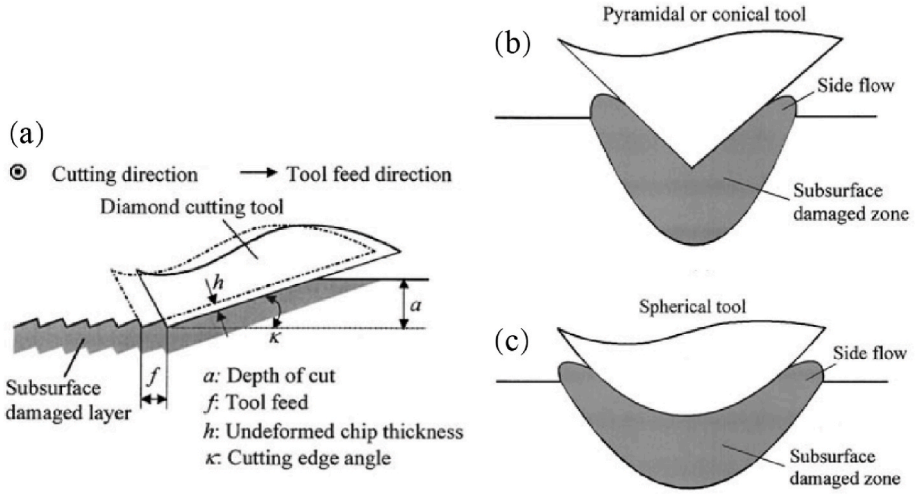

Fig. 28. Schematic of the subsurface damage layer produced by (a) single-point diamond turning, and nanoindentation using (b) conical/pyramidal and (c) spherical indenters [86].

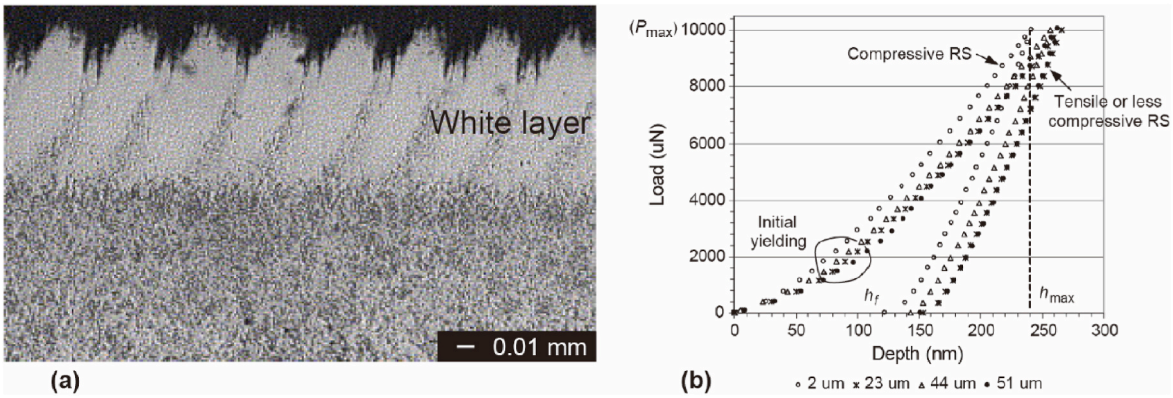

Fig. 29. (a) Cross-sectional image of a white layer in a turned surface of AISI 52100 steel, and (b) the load-displacement curves for the indents performed on the sample cross-section [94].

decreased due to the formation of subsurface damages, i.e., an amorphous silicon layer. When performing indention on pristine silicon, only elbow appears on the unloading part of the curve, as shown in Fig. 3(a), which suggesting a transformation from diamond cubic structure to amorphous. However, for the machined silicon under the same conditions, pop-in phenomenon occurs during loading, meanwhile a pop-out occurs during unloading, as shown in Fig. 30(b). The pop-in and pop-out occurring in the indentation of machined silicon might be caused by a further phase transformation of the amorphous silicon. The hardness values of pristine silicon and machined silicon under varied indentation loads are summarized in Fig. 30(c). In general, as the indentation load increases, although the hardness of both samples is decreased due to the indentation size effect, the hardness of machined silicon gradually aligns with that of pristine silicon. Therefore, by conducting a series of indentation tests on both pristine and machined samples with progressively large indentation loads, the thickness of subsurface damage layer can be estimated.

3.1.2. Plastic deformation and fracture behaviour

Combining nanoindentation tests with SEM observation or surface topography measurements allows evaluation of the ductility/plasticity of a machining-induced subsurface damaged layer. If the subsurface damage layer is more ductile than the material substrate, it can be identified by the height and size of the surface pileup after the indentation. A typical example is the indentation on amorphous silicon layer produced in diamond turning of single crystal silicon. Fig. 31(a) and (b) present the surface topographies and cross-sectional profiles of the residual indents on the pristine silicon and machined silicon, respectively, which are measured by atomic force microscope (AFM) [95]. From the indent profile of pristine silicon, it can be seen that the indented surface is connected to the sample surface by a smooth transition, showing no evidence of protrusions; while from the indent profile of machined silicon, there is significant protrusion around the indent, which demonstrates that the amorphous layer has been subjected to significant plastic flow during indentation. Thus, it can be inferred that when the indenter is loaded on pristine silicon, the high-pressure phase is constrained below the indenter by the near-surface diamond-cubic phase and cannot escape to the free surface to generate protrusions; whereas when the indenter is loaded on the machined silicon, due to the existence of amorphous layer in which the atoms are easier to rearrange, the high-pressure phase can extend to the free surface, forming a pathway allowing the material to be extruded out from under the indenter. Therefore, it can be inferred that the formation of the amorphous phase with a good microplasticity in the machined subsurface of silicon would improve the ductile machinability of silicon, because when processing silicon wafers, the tool will always remove the amorphous silicon formed in the previous cut and produce new amorphous phase in the subsurface simultaneously. As the amorphous layer is usually formed in the last cut this influences the surface function of produced silicon parts.

If the machining-induced subsurface damage layer is more brittle

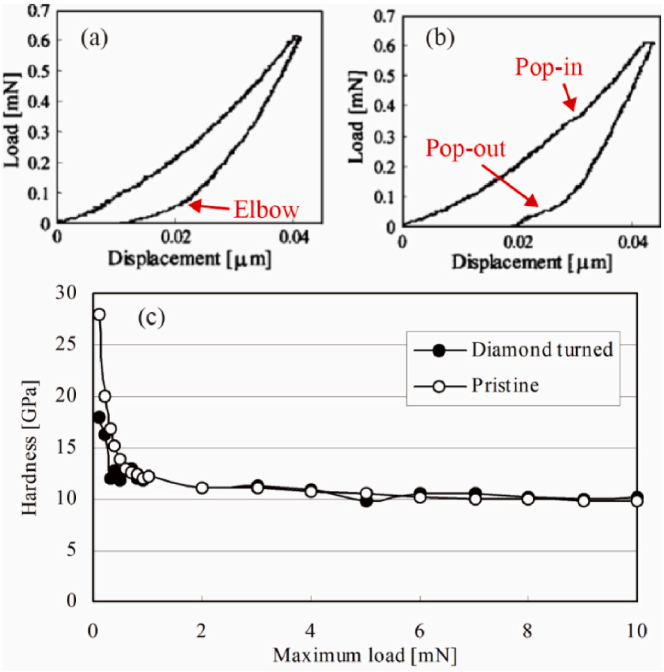

Fig. 30. Typical load-displacement curves for nanoindentation tests on (a) chemo-mechanical polished silicon wafer, and (b) diamond-turned silicon wafer. (c) Comparison of measured hardness between the pristine silicon and the machined silicon [95]. (For interpretation of the references to colour in this figure legend, the reader is referred to the Web version of this article.)

than the material substrate before machining, it can be identified by the crack generation after the indentation. A typical example is the indentation on grain refinement layer produced in diamond turning of zirconia polycrystal. Fig. 32(a) and (b) present the surface morphologies of the residual indents on the unmachined and machined zirconia poly crystal, respectively, which are observed by scanning electron microscope (SEM) [96]. For the residual indent on the unmachined surface, the three planes of the indent are smoother than the raw surface due to the pressing by indenter, but no brittle fractures are observed. On the raw surface around indented planes, grain boundaries are clearly seen, although grain boundaries become blurred near the indent centers and edges. These results suggest significant plastic deformation of the crystal grains due to the pressing of the indenter faces. For the residual indent on the machined surface, although the three planes of the indent are smooth without any fractures, cracks are generated around the indented planes. Moreover, it is found that the cracks are generated along the direction perpendicular to the cutting direction. This may imply that a residual tensile stress is formed along the cutting direction in the workpiece subsurface when diamond-turning, which consequently will lead to a decreased threshold of fracture toughness for the machined surface.

3.1.3. *Subsurface structural change*

By combining nanoindentation tests and cross-sectional transmission electron microscope (X-TEM) observation, the responses of the subsurface regions of the workpiece before and after machining to mechanical loads can be visualized. Fig. 33(a) and (b) show X-TEM images of indents made on pristine silicon samples under the indentation loads of 20 mN and 50 mN [97]. In these two images, the dotted lines abc show the indented surfaces after unloading, and just below the indented surfaces, light grey regions indicated by abcd can be identified. For the indent produced at 20 mN, the material in the region abcd shows a uniform amorphous phase. For the indent produced at 50 mN, the depth of amorphous region abcd has increased and a median crack initiate downward from the bottom of the amorphous region; moreover, numerous nano crystal grains form within the amorphous phase. Fig. 33 (c) shows a subsurface damage layer with amorphous silicon caused by diamond turning. Then, the two indents are produced at the loads of 20 and 50 mN on this machined silicon sample, as shown in Fig. 33(d) and (e) [98]. For the indent produced at 20 mN, the amorphous region right below the indenter tip becomes apparently thicker than the machining-induced amorphous layer, indicating that the existing amorphous layer has been penetrated by the indenter and a new amorphous zone is formed by the indentation. However, the size of the amorphous region formed in the subsurface of machined silicon is smaller than that formed in pristine silicon subsurface. On the left side of the indent, which corresponds to one of the faces of the indenter, a protrusion caused by the side flow of the amorphous silicon is formed, which not be observed on the pristine silicon sample. This indicates that the machining-induced subsurface layer disperses the contact pressure to the free surface of the workpiece in the form of plastic flow, leading to a smaller amorphous region beneath the indenter. For the indent

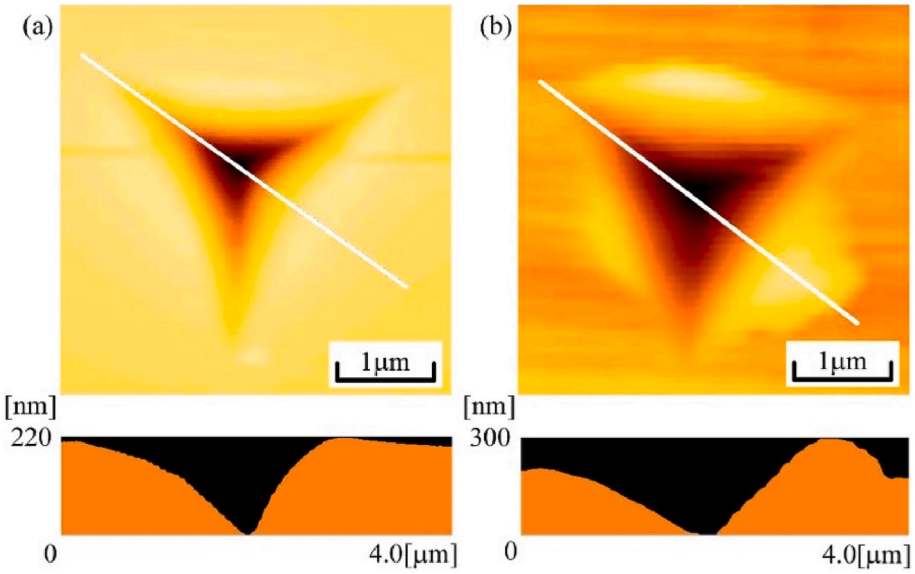

Fig. 31. AFM topographies and cross-sectional profiles of indents generated on (a) pristine silicon and (b) machined silicon [95]. (For interpretation of the references to colour in this figure legend, the reader is referred to the Web version of this article.)

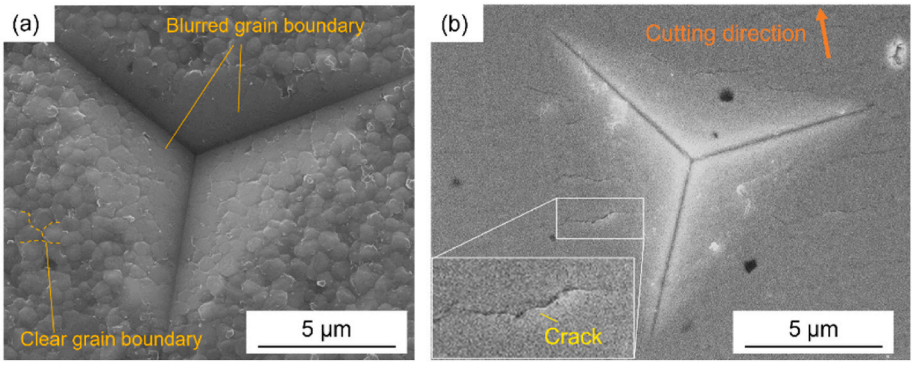

Fig. 32. SEM images of indents performed on the (a) unmachined surface, and (b) machined surface of zirconia poly crystal [96].

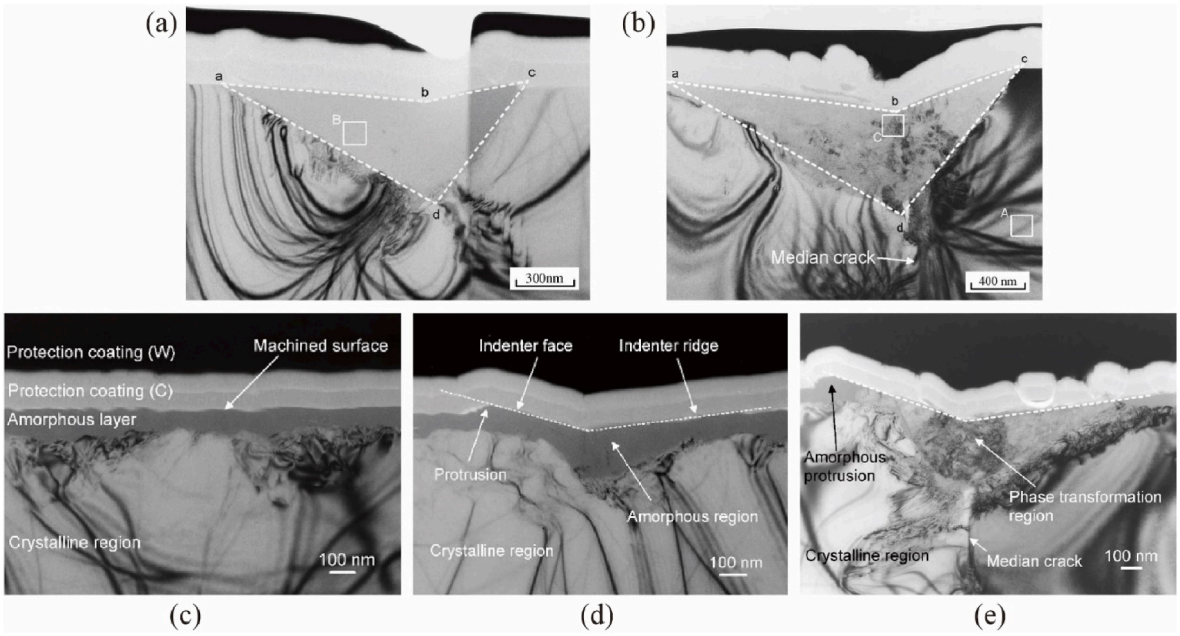

Fig. 33. X-TEM images of the indents made on pristine silicon sample under the indentation loads of (a) 20 mN, and (b) 50 mN [14]. X-TEM images of (c) the amorphous layer formed in the subsurface of diamond-machined silicon; the indents made on the machined silicon sample under the indentation loads of (d) 20 mN, and (e) 50 mN [98].

produced at 50 mN, the microstructure of the material within the region right below the indenter tip exhibits significant heterogeneity, though the side protrusion and machined subsurface damage layer still remain to be uniform amorphous state. This suggests that a relative high load could cause recrystallization of the machining-induced amorphous silicon, while the recrystallization is insignificant under small load conditions.

3.1.4. Surface/subsurface evolution under cyclic loading/unloading

As aforementioned in Section 3.1.3, the microstructure of the machining-induced subsurface damages undergoes further changes when it subjects to a mechanical load. In practical applications, mechanical parts are often subjected to repeated impacts. How the subsurface damage layer evolves under repeated loading can be investigated by cyclic nanoindentation experiments. The time-load curve for a typical cyclic nanoindentation is illustrated in Fig. 34(a) [96]. In this case, the identical indenter loading/unloading procedure is repeated ten times in the same position on the sample. Fig. 34(b) and (c) present the surface morphologies of the residual indents on the unmachined and machined zirconia poly crystal under ten cycles cyclic nanoindentation [96]. For the residual indents produced on the unmachined surface, the morphologies of the indents under single indentation (see Fig. 32(a)) and cyclic indentation (see Fig. 34(b)) are similar; while for the residual indents produced on the machined surface, under cyclic indentation a crater is formed due to the material is spalling from the substrate. This might be because cyclic indentation could induce microcracks along the interface between the grain-refinement layer and the substrate. Then the microcracks propagate, resulting in spalling of the grain-refinement layer, as schematically shown in Fig. 35.

It must be pointed out that most of the nanoindentation characterizations discussed here are post-mortem tests. There are scarcely in-situ technologies for these characterizations yet. However, the surface properties like hardness and plastic deformation need the in-situ characterisation in machining, like the on-machine characterisation of surface roughness and form accuracy. If in-situ characterisation of surface hardness and plasticity realized, the on-machine feedback control of these surface properties might become possible.

3.2. Micro-pillar and cantilever beam test of machined surface layer

Micro/nano scale mechanics test has been developed rapidly in the past decades for testing the small-scale mechanical performance of materials including hardness, elastic modules, strength, fracture toughness as well as their fundamental deformation mechanisms [42].

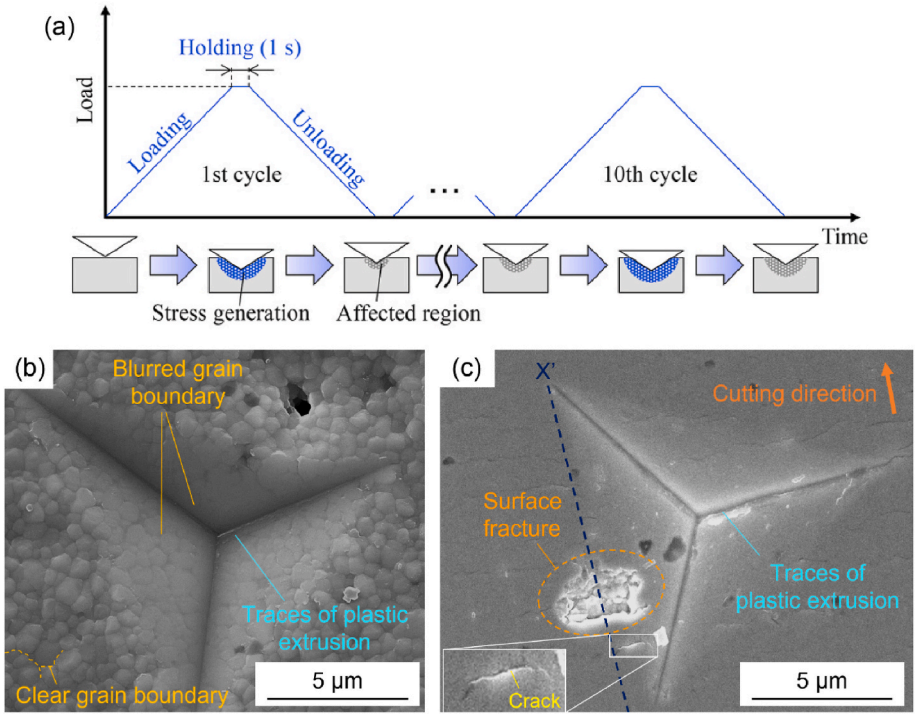

Fig. 34. (a) Schematic of time-load curve for cyclic nanoindentation. SEM images of the indents performed on the (a) unmachined surface, and (b) machined surface of zirconia poly crystal. Ten cycles cyclic nanoindentation with the maximum load of 1000 mN [96].

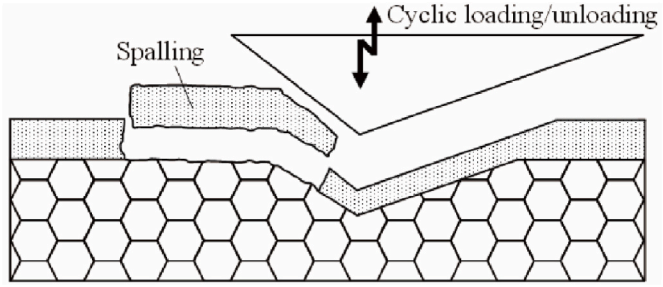

Fig. 35. Schematic diagram of material spalling from the substrate [96].

These tests normally include indentation, micropillar compression and cantilever bending [99]. While micro/nano indentation has already been widely used for characterising the hardness, elastic modules and fracture toughness of machined surface, micro-pillar and cantilever tests are relatively new and rarely used in machining applications. Compared with indentation test whereby the yielded stress-strain field depends on the geometry of specific indenter tip, micro-pillars and cantilevers can gain a relatively uniform stress-strain field through careful geometrical design and fabrication. Hence, this technology has the potential to be employed for characterise the uniaxial stress-strain constitutive relation of the materials at small scales before and after machining [100]. To the knowledge of the authors, Liao et al. [101] were the first one in the machining community to employ the micro-pillar test to characterise the properties of machined surface layer, and recently this technology became more and more popular in machining community [102–104].

The machining induced surface defects are normally at relatively small scale. For instance, the thickness of machining induced white layer can be less than 5 μm, as shown in Fig. 36 [104]. This makes it difficult to extract the mechanical performance of the machining induced surface modification from the bulk material through conventional macro mechanical test. On the other hand, while the micropillar and cantilever beam tests allow the study of the material property/mechanical behaviour at a micro scale, the key factor is to define a proper micro geometry that dimensionally matches the machining induced surface defects. In general, the size of a pillar (e.g. 3 μm diameter and 9 μm height) can be much smaller than grain size (10 μm) in bulk material while much bigger than that in white layer (100 nm grain size) [101], as shown in Fig. 37. In other words, if micropillar were machined from the bulk, it may include only one or few grains, thus their strength can also be influenced from the Hall-Petch effect and grain orientation compared to bulk material [102].

Thanks to the uniform stress-strain field underneath the indenter in a micropillar test, the strength of the thin machined layer can be achieved, eventually to reveal the materials strengthening mechanism in machining. That is, by using of unique micropillar compression tests, the superficial (recrystallized, dragged) layers generated during machining can be evaluated for their yield strength and deformation mechanism, thus giving the fundamental understanding on the nature of resulted surface integrity. As shown in Fig. 38, while the micropillar tested yield strength of bulk material in a Nickel based superalloy is similar to the conventional tensile tested results (~1000 MPa), the true stress-strain curves of machined surface shows that the yield strength of the white layer is ~2000 MPa, which is nearly twice of the bulk material [101]. More interestingly, it shows that the white layer fails in a buckling mode while the bulk material fails in a slipping mode. By employing the micropillar test, Liao et al. [101] for the first time were able to reveal the true strength of the white layer and its deformation mechanism at micro scale. Nevertheless, while the white layer is generally regarded as a deteriorated layer, the resulted higher strength seems cannot explain the material deterioration mechanism. In this sense, the strength evaluation of machined layer is not enough, and a further plasticity evaluation is required.

Hence, to study how the elastoplastic material mechanical properties change within the thin layer induced by the severe plastic deformation during the machining process, uniaxial cyclic loading-unloading compression tests of micro-pillars can also be performed on both the white layer and the bulk material. By prescribing the cyclic loading-unloading mode of the micro-pillar compression testing, the elastic

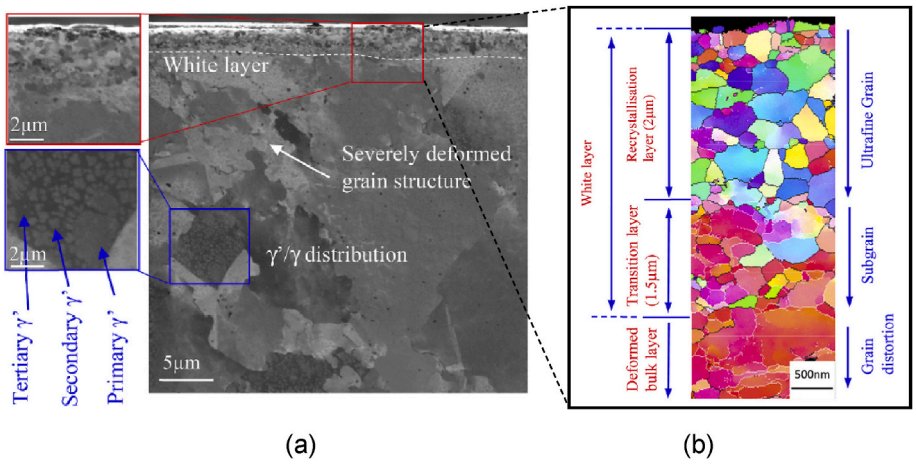

Fig. 36. Materials alternation layer at small scale, an example 3 μm thickness of white layer and its grain structure in machined Nickel based superalloy: (a) Ion contrast channelling imaging and (b) Transmission Kikuchi Diffraction imaging [104].

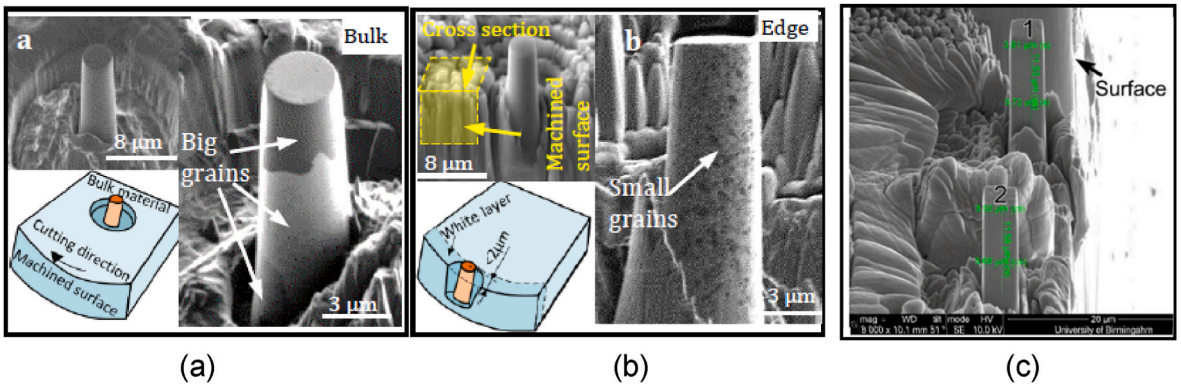

Fig. 37. Preparation of micropillars: (a) micropillar in bulk material that covers only 3 grains in the pillar and (b) micropillar within white layer that covers a number of grains, (c) square shape micropillar in the machined surface [101,102].

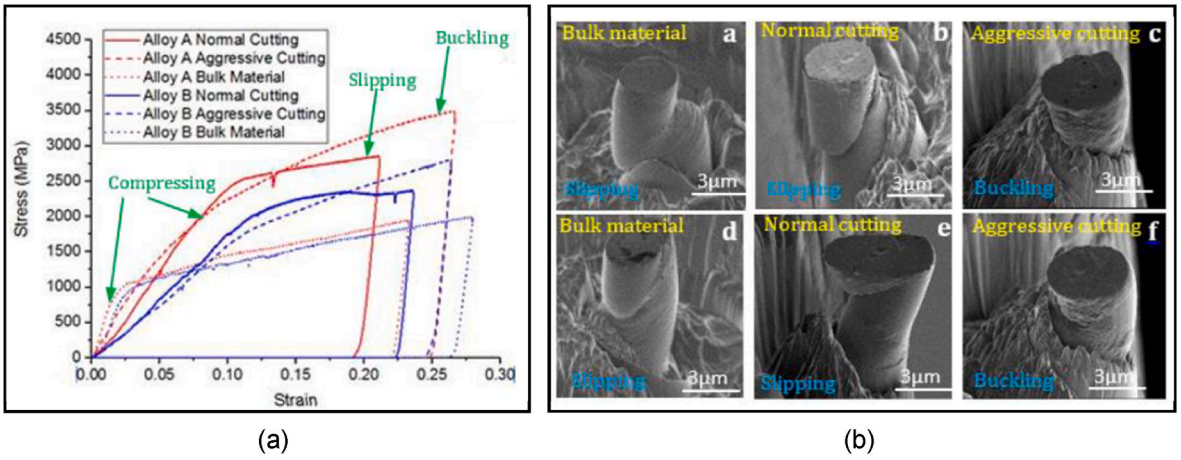

Fig. 38. Results of micropillar compression test in machined surface: (a) stress-strain curve, (b) pillar failure mode. The aggressive cutting represents white layer and normal cutting represents deformed layer [101].

and plastic energy can be achieved in each cycle and eventually revealing the materials deformation behaviour in an elastoplastic regime. The results in Fig. 39 shows that while a high elastic behaviour can be observed in bulk material under the yield stress, there is almost no elastic recovery even at low stresses (e.g. 300 MPa) of while layer. In contrast, a high plastic strain and energy has been revealed in white layer [104]. This significant plasticity fundamentally explains the deterioration of the material mechanical performance, which cannot be revealed under macro-mechanics test due to the interference of bulk material.

Similar to the study on Nickel based superalloy machining by Liao et al. [101], an enhanced strength were also found in the machined chip

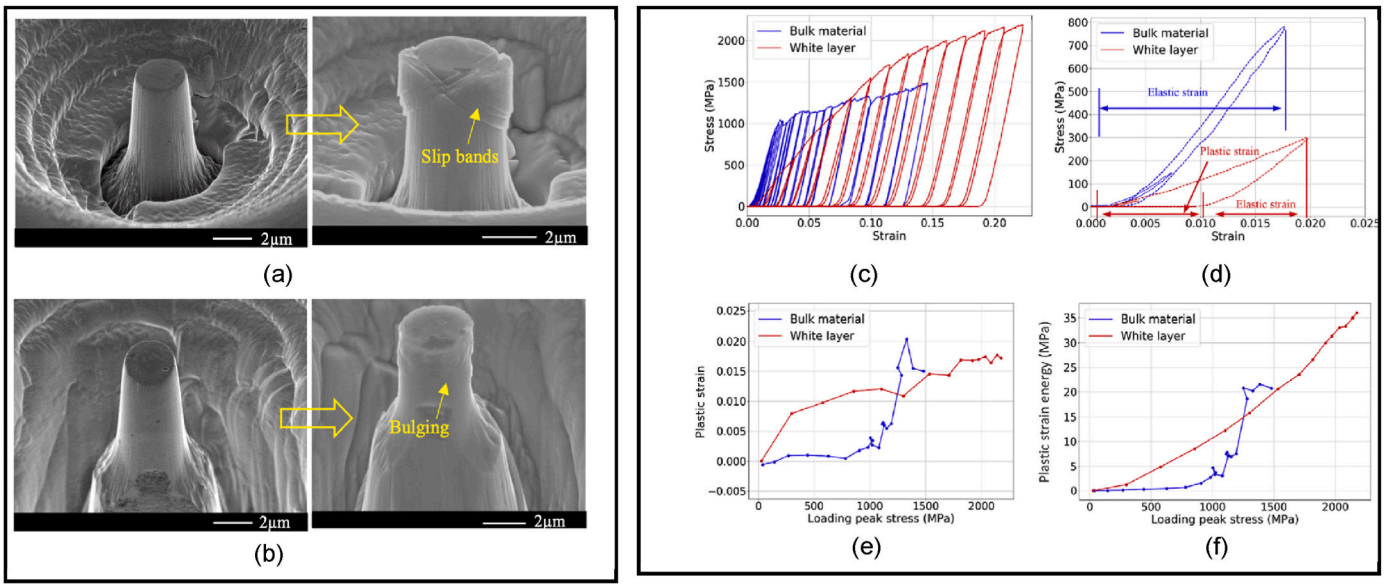

Fig. 39. Cyclic compression test of micro-pillars in the white layer and bulk material: (a) and (b) pillar deformation mode, (c) and (d) stress-strain curves of displacement controlled loading-unloading compression tests, (e) plastic strain and (f) plastic strain energy vs loading stress [104].

surface of pearlitic steel by Medina-Clavijo et al. [103]. Furthermore, they also studied different pillar sizes at various positions of superficial layer on the machined chip and found out that the pillar diameter does not make a notable influence on the strength, which indicates no size-effect of the pillar on their measurements. In contrast, the strength strongly depends on the distance to the chip edge, i.e. on the grain size and on the strain state of the material, as shown in Fig. 40.

Moreover, micro-pillar compression test, as an emerging technology for machined surface characterisation, cannot only fundamentally reveal the surface layer formation mechanism of engineering materials, but also provides a thorough understanding of the biological tissue (e.g., bone) deterioration mechanism when it is applied in surgical operations/machining [105,106]. Commonly, histology test is used to evaluate the necrotic/heat damage depth caused by machining into bone. Through micro-pillar compression test, Robles-Linares et al. for the first time revealed that the microstructure shifts from being ductile in the bulk, to brittle and mechanically weaker near the machined surface, as shown in Fig. 41 [105]. Moreover, this brittle layer is found can extend to around 1500 μm away from the machined surface, which is more than 3 times the necrotic depth measured from histology test. This interesting observation reveals that in tissue machining the mechanical deterioration of the tissues are different from histological ones and proves the need of micro-mechanics test to evaluate the machining induced damage of biological tissues.

On the other hand, while the micropillar test can only reveal the pillar deformation under compression mode, micro cantilever beam test can reveal the tensile deformation as well as fracture failure mechanism through bending test, as shown in Fig. 42. This is commonly applied to study the fracture behaviour of brittle materials while has also recently been employed to study the shear behaviour of ductile materials [105]. However, up to now this technology has been scarcely employed for machining induced surface layer test yet. While the materials can experience a tension state in the upper region and a compression state on the opposite side under cantilever beam bending test [107], this

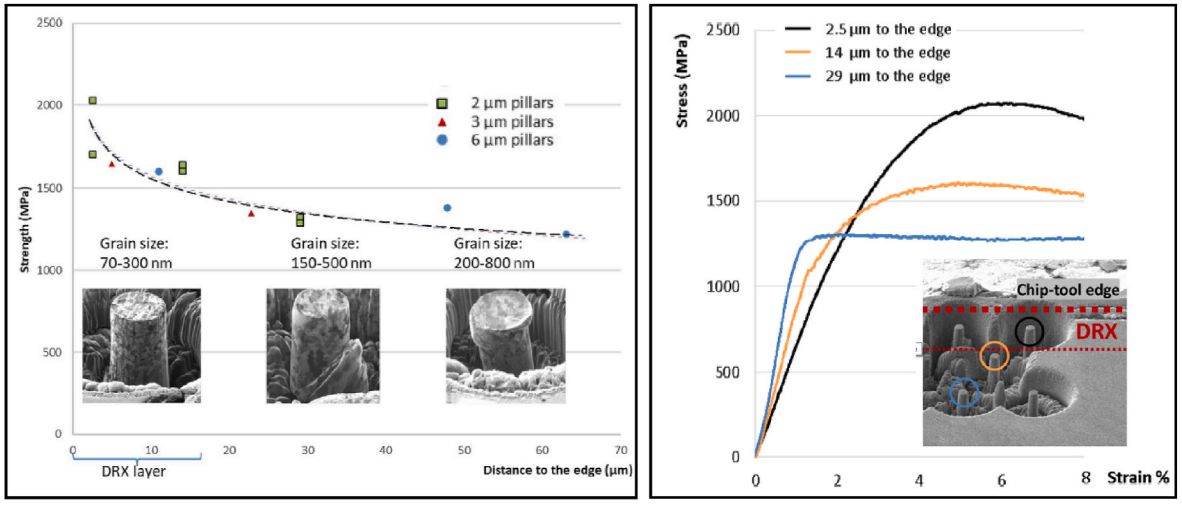

Fig. 40. (a) The pillar strength of the machined pearlitic steel chip vs distance to the chip edge, obtained by pillar compression tests of the pillars at 2, 3 and 6 μm of diameter; (b) stress–strain plot for 2 μm diameter pillars milled at 2.5, 14 and 29 μm from the chip edge.

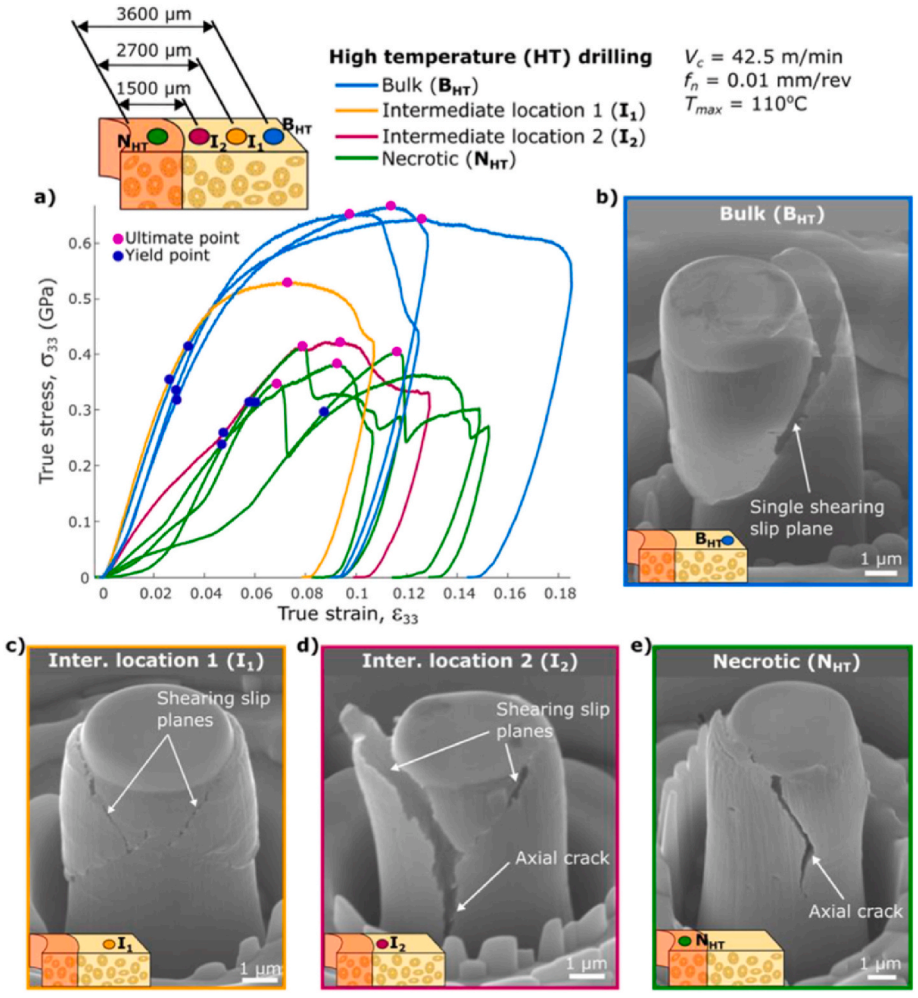

Fig. 41. Stress-strain curves and failure micrographs of micro-pillars of bone machining: (a) stress-strain curves shows the decreased strength in machined surface compare to bulk micro-pillars; (b) shows ductile failure mode in bulk material compared to brittle failure mode (c)–(e) in the machined subsurface [105].

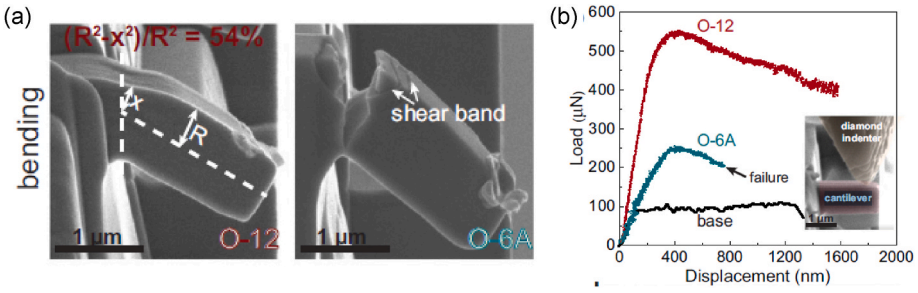

Fig. 42. Cantilever beam bending test of ductile material (TiNbZr–O–C–N MISS alloys) to study the shear behaviour under tension state: (a) SEM picture of cantilever beam, (b) load-displacement curves [107].

technology has the potential for machining induced surface damage evaluation.

To the knowledge of the authors, currently only Medina-Clavijo et al. [103] reported to use micro cantilever beam test to study machined process outcome. It is reported that cyclic cantilever beam bending can provide good sensitivity to modulus calculation while it is relatively indifferent to small geometric misalignments. As shown in Fig. 43, through the cantilever beam bending test, they achieved a quantified elastic modulus (i.e., 178 ± 5 GPa) for the DRX layer in the machined chip of AISI 1045 annealed steel, which is 12% less than the elastic modulus of pristine AISI1045. Combining with the micropillar test, they were able to measure the true strength and electric modulus of the machined layer and proved that the machining induced structure refinement makes the strength higher while also brings down the elastic modulus [103].

4. Future research avenues and conclusions

While some interesting research has been discussed in relation to the use of micro-mechanical testing systems for both studying the machining operations and the property alterations of workpiece surface, the authors believe there are still a significant number of exciting topics

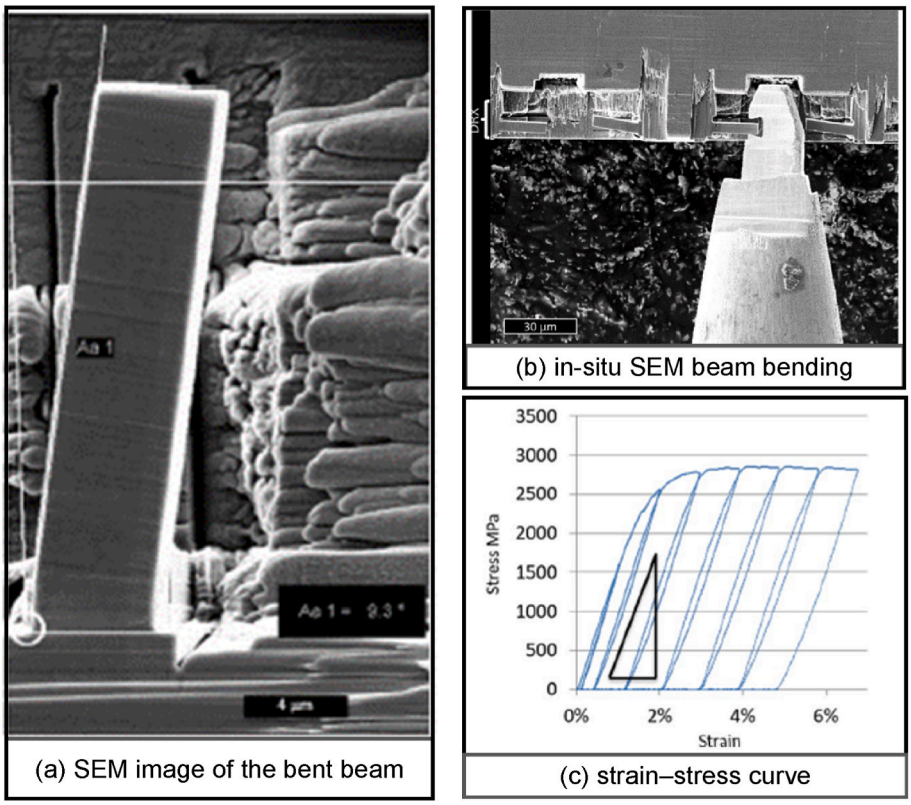

Fig. 43. Micro cantilever beam bending experiments for elastic modulus calculation of machined chip of AISI 1045. (a) SEM image of the bent beam; (b) Set-up for in-situ in the SEM cantilever beam bending experiments; (c) typical measured strain–stress curve for cantilever beam bending experiment.

that could be the subject of further studies, as listed below.

In-situ SEM high strain rate scratching/cutting: While some intimacies of machining process can be captured by low strain rate scratching/cutting on these micro-mechanical testing systems, there has always been a reservation to translate the findings to the real machining processes. However, the modern micro-mechanical testing systems are capable of performing relative movements between indenters/cutting tips and test pieces at high strain rates. These tests might reveal how the shear mechanism of single grains is affected by strain rate, which bridges the knowledge with the domain of crystal plasticity. Nevertheless, these tests can be performed at very limited strokes (i.e., micrometric level depending on the strain rate) which implies that the mimicked cutting/grinding (i.e., for scratching) process would not reach steady state (e.g. in chip formation, surface property alterations). Moreover, with such short strokes, the preparation of the experiments will also present some challenges, e.g., the cutting tool radius must be at nanometer level to allow full engagement of the edge on a traveling distance at the order of micrometre.

In-situ SEM quick-stop cutting: While quick-stop cutting tests have been used for decades for revealing the chip formation mechanism at macro-level, those studies have missed such process intimacies at micrometric level. Of course, such research goals might require additional axis to the existing in-situ micro-mechanical testing systems to enable fast retraction of the cutting edge from its engagement with the test piece or careful preparation of the sheared area of the sample (i.e., ahead of the cutting edge) so that it disengages with the bulk part of the sample. Both approaches have been reported on conventional machining setups but not on ultra-high precision and micrometric scale.

In-situ SEM high temperature cutting: While up to now the micro-mechanical testing systems have been used to mimic cutting processes, very limited attempts have been reported to perform these tests under different temperatures. This is possible since these systems can be equipped with high temperature (e.g.,1000 °C) modules to heat-up the test piece; such setup can be further enriched with Digital Image Correlation (DIC) which could provide additional information of the displacement of the grains that undergo stresses induced by cutting edge. Despite the uniform heating of the workpiece, that does not match the transient one happening during cutting, these tests can provide useful in-depth information on how the shear deformation within grains and grain boundaries are affected by varying temperatures which could lead to better understanding of the aspects on workpiece surface integrity as (sub)micrometre scales. Of course, the above approach could be applied to both low and high strain rate tests.

In-situ optical microscope cutting/scratching under controlled media: With the goal of performing the scratching/cutting tests under the generic framework of three body contact, i.e., presence of a cooling/lubrication media, the concept of "in-situ" needs to be translated from SEM to optical microscope environments; this should not be considered as a "less cool" approach since, nowadays, high resolution optical microscopes exist. In this train of thoughts, such experiments where solid and/or solid media can be delivered at the interface of the cutting edge with the workpiece counterpart to better understand how these influence the friction and heat dissipation phenomena at micro-scale.

All the above tests might be further advanced to perform more complex paths of the tips. Typically, the micro-mechanical testing systems, being developed mainly for material characterisation, enable the movement of a single stage at a time; nevertheless, the existing control systems would allow the simultaneous movement of 2–3 axis this will allow the cutting research community to extend these studies to resemble more the reach machining operations.

In-situ Atomic Force Microscope (AFM) scratching/cutting/milling: Although not performed with the previously described micro-mechanical testing systems, this technique enables micro/nanometric scratches as well as measurement of the surface. While many researches have been reported with the scope of mimicking machining operations, the great majority used the conventional (sharp) measurement tips at

very low displacement speeds. However, some avenues for addressing these aspects could be created by customising the geometry of the tips to resemble the real cutting edges as well as mounting on the AFM additional stages able of high velocities/accelerations. Of course, with such updates, there, contact forces between the tip and test piece are likely to increase and therefore, additional care on the setup preparation needs to be considered.

In-situ Transmission Electron Microscope (TEM) testing: This is a very special material characterisation technique by which very thin lamella can be extracted from a particular zone of the test piece and apply quasi-static/dynamic loads while observing the material deformation (e.g., motion of dislocations or twinning) at very high resolution. As it has been recently reported high strain rates (up to 10^4 s^{-1}) can be performed in-situ TEM. As these are values that are close to those experienced in cutting, if samples are prepared to enable controlled shear of material such approach could be of very high value to understand, at nanometric scale, how deformation evolves in cutting processes.

Credit author statemet

Dragos Axinte: Conceptualization, Investigation, Methodology, Writing – original draft & editing. **Han Huang**: Conceptualization, Investigation, Methodology, Writing – original draft & editing. **Jiwang Yan**: Conceptualization, Investigation, Methodology, Writing – original draft & editing. **Zhirong Liao**: Conceptualization, Investigation, Methodology, Writing – original draft & editing.

Declaration of competing interest

The authors declare that they have no known competing financial interests or personal relationships that could have appeared to influence the work reported in this paper.

Data availability

Data will be made available on request.

References

[1] Z. Liao, A. la Monaca, J. Murray, A. Speidel, D. Ushmaev, A. Clare, D. Axinte, R. M'Saoubi, Surface integrity in metal machining - Part I: fundamentals of surface characteristics and formation mechanisms, Int. J. Mach. Tool Manufact. 162 (2021), https://doi.org/10.1016/j.ijmachtools.2020.103687.

[2] A. la Monaca, J.W. Murray, Z. Liao, A. Speidel, J.A. Robles-Linares, D.A. Axinte, M.C. Hardy, A.T. Clare, Surface integrity in metal machining-Part II: functional performance, Int. J. Mach. Tool Manufact. (2021), 103718.

[3] T.H.C. Childs, A new visio-plasticity technique and a study of curly chip formation, Int. J. Mech. Sci. 13 (1971), https://doi.org/10.1016/0020-7403(71)90061-0.

[4] R. Komanduri, Some clarifications on the mechanics of chip formation when machining titanium alloys, Wear 76 (1982) 15–34, https://doi.org/10.1016/0043-1648(82)90113-2.

[5] A. la Monaca, D.A. Axinte, Z. Liao, R. M'Saoubi, M.C. Hardy, Towards understanding the thermal history of microstructural surface deformation when cutting a next generation powder metallurgy nickel-base superalloy, Int. J. Mach. Tool Manufact. 168 (2021), 103765.

[6] A. Malakizadi, T. Hajali, F. Schulz, S. Cedergren, J. Ålgårdh, R. M'Saoubi, E. Hryha, P. Krajnik, The role of microstructural characteristics of additively manufactured Alloy 718 on tool wear in machining, Int. J. Mach. Tool Manufact. 171 (2021), 103814.

[7] J. Schoop, D. Adeniji, I. Brown, Computationally efficient, multi-domain hybrid modeling of surface integrity in machining and related thermomechanical finishing processes, Procedia CIRP 82 (2019) 356–361, https://doi.org/10.1016/J.PROCIR.2019.03.225.

[8] B. Wang, Z. Liu, Y. Cai, X. Luo, H. Ma, Q. Song, Z. Xiong, Advancements in material removal mechanism and surface integrity of high speed metal cutting: a review, Int. J. Mach. Tool Manufact. 166 (2021), 103744.

[9] H. Kolsky, An investigation of the mechanical properties of materials at very high rates of loading, Proc. Phys. Soc. B 62 (1949) 676, https://doi.org/10.1088/0370-1301/62/11/302.

[10] J. Ellis, R. Kirk, G. Barrow, The development of a quick-stop device for metal cutting research, Int. J. Mach. Tool Des. Res. 9 (1969) 321–339, https://doi.org/10.1016/0020-7357(69)90007-9.

[11] O. Vingsbo, Experimental studies of shear zones during chip formation in metal cutting, J. Phys. Colloq. 46 (1985), https://doi.org/10.1051/jphyscol:1985547i.

[12] G. Feng, D. Sagapuram, A strong basis for friction as the origin of size effect in cutting of metals, Int. J. Mach. Tool Manufact. 168 (2021), 103741.

[13] D. Xu, Z. Liao, D. Axinte, M. Hardy, A novel method to continuously map the surface integrity and cutting mechanism transition in various cutting conditions, Int. J. Mach. Tool Manufact. (2020), 103529.

[14] H. Huang, X. Li, D. Mu, B.R. Lawn, Science and art of ductile grinding of brittle solids, Int. J. Mach. Tool Manufact. 161 (2021), https://doi.org/10.1016/J.IJMACHTOOLS.2020.103675.

[15] M. Harzallah, T. Pottier, R. Gilblas, Y. Landon, M. Mousseigne, J. Senatore, A coupled in-situ measurement of temperature and kinematic fields in Ti-6Al-4V serrated chip formation at micro-scale, Int. J. Mach. Tool Manufact. 130–131 (2018) 20–35, https://doi.org/10.1016/J.IJMACHTOOLS.2018.03.003.

[16] A. la Monaca, Z. Liao, D.A. Axinte, R. M'Saoubi, M.C. Hardy, Can higher cutting speeds and temperatures improve the microstructural surface integrity of advanced Ni-base superalloys? CIRP Ann 71 (2022) 113–116, https://doi.org/10.1016/J.CIRP.2022.04.061.

[17] (n.d.), https://alemnis.com/.

[18] D. Tabor, The Hardness of Metals, Clarendon, Oxford, 1951.

[19] B.R. Lawn, A.G. Evans, D.B. Marshall, Elastic/plastic indentation damage in ceramics: the median/radial crack system, J. Am. Ceram. Soc. 63 (1980) 574–581, https://doi.org/10.1111/J.1151-2916.1980.TB10768.X.

[20] B.R. Lawn, E.R. Fuller, NBSIR 75-730 Equilibrium Penny-Like Crack in Indentation Fracture, (n.d.). https://doi.org/10.6028/NBS.IR.75-730.

[21] R.F. Cook, A critical evaluation of indentation crack lengths in air, J. Am. Ceram. Soc. 103 (2020) 2278–2295. https://doi.org/10.1111/JACE.16925.

[22] B.R. Lawn, H. Huang, M. Lu, Ó. Borrero-López, Y. Zhang, Threshold damage mechanisms in brittle solids and their impact on advanced technologies, Acta Mater. 232 (2022), 117921, https://doi.org/10.1016/J.ACTAMAT.2022.117921.

[23] B.R. Lawn, O. Borrero-Lopez, H. Huang, Y. Zhang, Micromechanics of machining and wear in hard and brittle materials, J. Am. Ceram. Soc. 104 (2021) 5–22, https://doi.org/10.1111/JACE.17502.

[24] D. Axinte, P. Butler-Smith, C. Akgun, K. Kolluru, On the influence of single grit micro-geometry on grinding behavior of ductile and brittle materials, Int. J. Mach. Tool Manufact. 74 (2013) 12–18, https://doi.org/10.1016/J.IJMACHTOOLS.2013.06.002.

[25] T.G. Bifano, T.A. Dow, R.O. Scattergood, Ductile-regime grinding: a new technology for machining brittle materials, J. Eng. Ind. 113 (1991) 184–189, https://doi.org/10.1115/1.2899676.

[26] Y. Sun, D. Zuo, Y. Zhu, J. Li, Use of nanoindentation and nanoscratching tests to characterize the ductile-brittle transition, Adv. Sci. Lett. 4 (2011) 880–884, https://doi.org/10.1166/ASL.2011.1644.

[27] H. Huang, B.R. Lawn, R.F. Cook, D.B. Marshall, Critique of materials-based models of ductile machining in brittle solids, J. Am. Ceram. Soc. 103 (2020) 6096–6100, https://doi.org/10.1111/JACE.17344.

[28] Y. Wu, Deformation Mechanisms of Semiconductor Materials under Nanoscratching and Nanogrinding, PhD Thesis, University of queensland, 2011.

[29] Y. Wu, D. Mu, H. Huang, Deformation and removal of semiconductor and laser single crystals at extremely small scales, Int. J. Extrem. Manuf. 2 (2020), 012006, https://doi.org/10.1088/2631-7990/AB7A2A.

[30] Y.Q. Wu, H. Huang, J. Zou, J.M. Dell, Nanoscratch-induced deformation of single crystal silicon, J. Vac. Sci. Technol. B Microelectron. Nanom. Struct. Process. Meas. Phenom. 27 (2009) 1374, https://doi.org/10.1116/1.3049517.

[31] H. Huang, B.L. Wang, Y. Wang, J. Zou, L. Zhou, Characteristics of silicon substrates fabricated using nanogrinding and chemo-mechanical-grinding, Mater. Sci. Eng. 479 (2008) 373–379, https://doi.org/10.1016/J.MSEA.2007.06.061.

[32] K. Mylvaganam, L.C. Zhang, Nanotwinning in monocrystalline silicon upon nanoscratching, Scripta Mater. 65 (2011) 214–216, https://doi.org/10.1016/J.SCRIPTAMAT.2011.04.012.

[33] Y.Q. Wu, H. Huang, J. Zou, L.C. Zhang, J.M. Dell, Nanoscratch-induced phase transformation of monocrystalline Si, Scripta Mater. 63 (2010) 847–850, https://doi.org/10.1016/J.SCRIPTAMAT.2010.06.034.

[34] M. Wang, W. Wang, Z. Lu, Anisotropy of machined surfaces involved in the ultra-precision turning of single-crystal silicon—a simulation and experimental study, Int. J. Adv. Manuf. Technol. 60 (2011) 473–485, https://doi.org/10.1007/S00170-011-3633-7.

[35] H. Gao, X. Wang, D. Guo, Y. Chen, Research progress on ultra-precision machining technologies for soft-brittle crystal materials, Front. Mech. Eng. 12 (2017) 77–88, https://doi.org/10.1007/S11465-017-0411-8.

[36] S. Wang, C. An, F. Zhang, J. Wang, X. Lei, J. Zhang, An experimental and theoretical investigation on the brittle ductile transition and cutting force anisotropy in cutting KDP crystal, Int. J. Mach. Tool Manufact. 106 (2016) 98–108, https://doi.org/10.1016/J.IJMACHTOOLS.2016.04.009.

[37] W.J. Zong, Z.M. Cao, C.L. He, C.X. Xue, Theoretical modelling and FE simulation on the oblique diamond turning of ZnS crystal, Int. J. Mach. Tool Manufact. 100 (2016) 55–71, https://doi.org/10.1016/J.IJMACHTOOLS.2015.10.002.

[38] R. Irwan, H. Huang, H.Y. Zheng, H. Wu, Mechanical properties and material removal characteristics of soft-brittle HgCdTe single crystals, Mater. Sci. Eng. 559 (2013) 480–485, https://doi.org/10.1016/J.MSEA.2012.08.129.

[39] Z. Zhang, Y. Wu, H. Huang, New deformation mechanism of soft-brittle CdZnTe single crystals under nanogrinding, Scripta Mater. 63 (2010) 621–624, https://doi.org/10.1016/J.SCRIPTAMAT.2010.05.043.

[40] H. Wang, O. Riemer, K. Rickens, E. Brinksmeier, On the mechanism of asymmetric ductile–brittle transition in microcutting of (111) CaF2 single

crystals, Scripta Mater. 114 (2016) 21–26, https://doi.org/10.1016/J.SCRIPTAMAT.2015.11.030.
[41] Y. Zhang, L. Zhang, M. Liu, F. Zhang, K. Mylvaganam, W. Liu, Understanding the friction and wear of KDP crystals by nanoscratching, Wear 332–333 (2015) 900, https://doi.org/10.1016/J.WEAR.2014.11.032. –906.
[42] Q. Liu, Z. Liao, D. Axinte, Temperature effect on the material removal mechanism of soft-brittle crystals at nano/micron scale, Int. J. Mach. Tool Manufact. (2020), 103620.
[43] J. Zhang, D. Wang, P. Feng, Z. Wu, C. Zhang, Material removal characteristics of KDP crystal in ultrasonic vibration-assisted scratch process, Mater. Manuf. Process. 31 (2016) 1037–1045, https://doi.org/10.1080/10426914.2015.1070423.
[44] S. Yang, L. Zhang, Z. Wu, An investigation on the nano-abrasion wear mechanisms of KDP crystals, Wear 476 (2021), 203692, https://doi.org/10.1016/J.WEAR.2021.203692.
[45] Q. Liu, Z. Liao, J. Cheng, D. Xu, M. Chen, Mechanism of chip formation and surface-defects in orthogonal cutting of soft-brittle potassium dihydrogen phosphate crystals, Mater. Des. (2021), 109327.
[46] Y.Q. Wu, H. Huang, J. Zou, Transmission electron microscopy characterization of the deformation of CdZnTe single crystals induced by nanoscratching, Scripta Mater. 65 (2011) 392–395, https://doi.org/10.1016/J.SCRIPTAMAT.2011.05.008.
[47] H. Zhou, S. Qiu, X. Zhang, C. Xu, Mechanical characteristics of soft-brittle HgCdTe single crystals investigated using nanoindentation and nanoscratching, Appl. Surf. Sci. 258 (2012) 9756–9761, https://doi.org/10.1016/J.APSUSC.2012.06.026.
[48] J. Cao, Y. Wu, D. Lu, M. Fujimoto, M. Nomura, Material removal behavior in ultrasonic-assisted scratching of SiC ceramics with a single diamond tool, Int. J. Mach. Tool Manufact. 79 (2014) 49–61, https://doi.org/10.1016/J.IJMACHTOOLS.2014.02.002.
[49] X. Rao, F. Zhang, X. Luo, F. Ding, Y. Cai, J. Sun, H. Liu, Material removal mode and friction behaviour of RB-SiC ceramics during scratching at elevated temperatures, J. Eur. Ceram. Soc. 39 (2019) 3534–3545, https://doi.org/10.1016/J.JEURCERAMSOC.2019.05.015.
[50] W. Li, W. Liu, F. Qi, Y. Chen, Z. Xing, Determination of micro-mechanical properties of additive manufactured alumina ceramics by nanoindentation and scratching, Ceram. Int. 45 (2019) 10612–10618, https://doi.org/10.1016/J.CERAMINT.2019.02.128.
[51] G. Qiao, S. Yi, W. Zheng, M. Zhou, Material removal behavior and crack-inhibiting effect in ultrasonic vibration-assisted scratching of silicon nitride ceramics, Ceram. Int. 48 (2022) 4341–4351, https://doi.org/10.1016/J.CERAMINT.2021.10.229.
[52] G. Subhash, M. Klecka, Ductile to brittle transition depth during single-grit scratching on alumina ceramics, J. Am. Ceram. Soc. 90 (2007) 3704–3707, https://doi.org/10.1111/J.1551-2916.2007.01970.X.
[53] H.H.K. Xu, S. Jahanmir, Microfracture and material removal in scratching of alumina, J. Mater. Sci. 30 (1995) 2235–2247, https://doi.org/10.1007/BF01184566.
[54] H. Huang, Y.C. Liu, Experimental investigations of machining characteristics and removal mechanisms of advanced ceramics in high speed deep grinding, Int. J. Mach. Tool Manufact. 43 (2003) 811–823, https://doi.org/10.1016/S0890-6955(03)00050-6.
[55] A.W. Ruff, H. Shin, C.J. Evans, Damage processes in ceramics resulting from diamond tool indentation and scratching in various environments, Wear 181–183 (1995) 551–562, https://doi.org/10.1016/0043-1648(95)90171-X.
[56] K. Lee, K.P. Marimuthu, C.L. Kim, H. Lee, Scratch-tip-size effect and change of friction coefficient in nano/micro scratch tests using XFEM, Tribol. Int. 120 (2018) 398–410, https://doi.org/10.1016/J.TRIBOINT.2018.01.003.
[57] N. Bensaid, S. Benbahouche, F. Roumili, J.C. Sangleboeuf, J.B. Le Cam, T. Rouxel, Influence of the normal load of scratching on cracking and mechanical strength of soda-lime-silica glass, J. Non-Cryst. Solids 483 (2018) 65–69, https://doi.org/10.1016/J.JNONCRYSOL.2018.01.004.
[58] E. Shamoto, N. Suzuki, Ultrasonic vibration diamond cutting and ultrasonic elliptical vibration cutting, Compr. Mater. Process. 11 (2014) 405–454, https://doi.org/10.1016/B978-0-08-096532-1.01111-0.
[59] B. Lin, S. peng Li, Z.C. Cao, Y. Zhang, X.M. Jiang, Theoretical modeling and experimental analysis of single-grain scratching mechanism of fused quartz glass, J. Mater. Process. Technol. 293 (2021), 117090, https://doi.org/10.1016/J.JMATPROTEC.2021.117090.
[60] J. Feng, X. Huang, S. Yang, J. Qing, P. Tang, Z. Wan, Speed effect on the material behavior in high-speed scratching of BK7 glass, Ceram. Int. 47 (2021) 19978–19988, https://doi.org/10.1016/J.CERAMINT.2021.04.008.
[61] J. Yan, T. Asami, H. Harada, T. Kuriyagawa, Crystallographic effect on subsurface damage formation in silicon microcutting, CIRP Ann 61 (2012) 131–134, https://doi.org/10.1016/J.CIRP.2012.03.070.
[62] Z. Wang, J. Zhang, J. Zhang, G. Li, H. Zhang, H. ul Hassan, A. Hartmaier, Y. Yan, T. Sun, Towards an understanding of grain boundary step in diamond cutting of polycrystalline copper, J. Mater. Process. Technol. 276 (2020), 116400, https://doi.org/10.1016/J.JMATPROTEC.2019.116400.
[63] W. Huang, D. Yu, M. Zhang, Q. Cao, J. Yao, Predictive cutting force model for ductile-regime machining of brittle materials, Int. J. Adv. Manuf. Technol. 98 (2018) 781–790, https://doi.org/10.1007/S00170-018-2273-6.
[64] F. Fang, B. Liu, Z. Xu, Nanometric cutting in a scanning electron microscope, Precis. Eng. 41 (2015) 145–152, https://doi.org/10.1016/J.PRECISIONENG.2015.01.009.
[65] K. Ueda, K. Iwata, K. Nakayama, Chip formation mechanism in single crystal cutting of β-brass, CIRP Ann 29 (1980) 41–46.
[66] D. Xu, T.E.J. Edwards, Z. Liao, X. Maeder, R. Ramachandramoorthy, M. Jain, J. Michler, D. Axinte, Revealing Nanoscale deformation mechanisms caused by shear-based material removal on individual grains of a Ni-based superalloy, Acta Mater. 212 (2021), 116929.
[67] B. Medina-Clavijo, G. Ortiz-de-Zarate, A. Sela, I.M. Arrieta, A. Fedorets, P. J. Arrazola, A. Chuvilin, In-SEM micro-machining reveals the origins of the size effect in the cutting energy, Sci. Rep. 11 (2021) 1–18.
[68] A. Aretz, L. Ehle, A. Haeusler, K. Bobzin, M. Öte, S. Wiesner, A. Schmidt, A. Gillner, R. Poprawe, J. Mayer, In situ investigation of production processes in a large chamber scanning electron microscope, Ultramicroscopy 193 (2018) 151–158, https://doi.org/10.1016/J.ULTRAMIC.2018.07.002.
[69] R.W. Armstrong, S.M. Walley, High strain rate properties of metals and alloys, Int. Mater. Rev. 53 (2013) 105–128, https://doi.org/10.1179/174328008X277795.
[70] G.T. Rusty Gray, High-strain-rate deformation: mechanical behavior and deformation substructures induced, Annu. Rev. Mater. Res. 42 (2012) 285–303, https://doi.org/10.1146/ANNUREV-MATSCI-070511-155034.
[71] Y. Yang, H. Li, Z. Liao, D. Axinte, W. Zhu, A. Beaucamp, Controlling of compliant grinding for low-rigidity components, Int. J. Mach. Tool Manufact. (2020), 103543.
[72] S. Nemat-Nasser, H. Deng, Strain-rate effect on brittle failure in compression, Acta Metall. Mater. 42 (1994) 1013–1024, https://doi.org/10.1016/0956-7151(94)90295-X.
[73] H.S. Bhat, A.J. Rosakis, C.G. Sammis, A micromechanics based constitutive model for brittle failure at high strain rates, J. Appl. Mech. Trans. ASME. 79 (2012), https://doi.org/10.1115/1.4005897/456016.
[74] E.J. Frankberg, J. Kalikka, F.G. Ferré, L. Joly-Pottuz, T. Salminen, J. Hintikka, M. Hokka, S. Koneti, T. Douillard, B. Le Saint, P. Kreiml, M.J. Cordill, T. Epicier, D. Stauffer, M. Vanazzi, L. Roiban, J. Akola, F. Di Fonzo, E. Levänen, K. Masenelli-Varlot, Highly ductile amorphous oxide at room temperature and high strain rate, Science 366 (2019) 864–869, https://doi.org/10.1126/SCIENCE.AAV1254/SUPPL_FILE/AAV1254S1.MP4, 80-.
[75] B. Zhang, J. Yin, The 'skin effect' of subsurface damage distribution in materials subjected to high-speed machining, Int. J. Extrem. Manuf. 1 (2019), 012007, https://doi.org/10.1088/2631-7990/AB103B.
[76] Y. Wang, X. Li, Y. Wu, D. Mu, H. Huang, The removal mechanism and force modelling of gallium oxide single crystal in single grit grinding and nanoscratching, Int. J. Mech. Sci. 204 (2021), 106562, https://doi.org/10.1016/J.IJMECSCI.2021.106562.
[77] B.R. Lawn, B.J. Hockey, S.M. Wiederhorn, Thermal effects in sharp-particle contact, J. Am. Ceram. Soc. 63 (1980) 356–358, https://doi.org/10.1111/J.1151-2916.1980.TB10746.X.
[78] P. Zhang, Y. Yuan, Z.H. Gao, Y.F. Gu, J. Li, J.B. Yan, X.F. Gong, J.T. Lu, X.B. Shi, B.Q. Fu, Strain-rate insensitive yield strength and deformation mechanisms of Ni-base superalloy CM247LC at 600° C, J. Alloys Compd. 862 (2021), 158478.
[79] J. Yan, J. Tamaki, K. Syoji, T. Kuriyagawa, Single-point diamond turning of CaF2 for nanometric surface, Int. J. Adv. Manuf. Technol. 24 (2004) 640–646, https://doi.org/10.1007/S00170-003-1747-2.
[80] W. Huang, J. Yan, Chip-free surface patterning of toxic brittle polycrystalline materials through micro/nanoscale burnishing, Int. J. Mach. Tool Manufact. 162 (2021), 103688, https://doi.org/10.1016/J.IJMACHTOOLS.2020.103688.
[81] W. Huang, J. Yan, Deformation behaviour of soft-brittle polycrystalline materials determined by nanoscratching with a sharp indenter, Precis. Eng. 72 (2021) 717–729, https://doi.org/10.1016/J.PRECISIONENG.2021.07.016.
[82] W. Huang, J. Yan, B. Karpuschewski, O. Riemer, Fundamental investigation of diamond cutting of micro V-shaped grooves on a polycrystalline soft-brittle material, J. Manuf. Mater. Process. 5 (2021) 17, https://doi.org/10.3390/JMMP5010017.
[83] Z. Wang, J. Zhang, Z. Xu, J. Zhang, H. ul Hassan, G. Li, H. Zhang, A. Hartmaier, F. Fang, Y. Yan, T. Sun, Crystal plasticity finite element modeling and simulation of diamond cutting of polycrystalline copper, J. Manuf. Process. 38 (2019) 187–195, https://doi.org/10.1016/J.JMAPRO.2019.01.007.
[84] J. Yan, Z. Zhang, T. Kuriyagawa, Effect of nanoparticle lubrication in diamond turning of reaction-bonded SiC, Int. J. Autom. Technol. 5 (2011) 307–312, https://doi.org/10.20965/IJAT.2011.P0307.
[85] H. Nili, K. Kalantar-Zadeh, M. Bhaskaran, S. Sriram, In situ nanoindentation: probing nanoscale multifunctionality, Prog. Mater. Sci. 58 (2013) 1–29, https://doi.org/10.1016/J.PMATSCI.2012.08.001.
[86] J. Yan, Laser micro-Raman spectroscopy of single-point diamond machined silicon substrates, J. Appl. Phys. 95 (2004) 2094, https://doi.org/10.1063/1.1639953.
[87] S. Roy, R. Kumar, A.K. Sahoo, A. Pandey, A. Panda, Investigation on hard turning temperature under a novel pulsating MQL environment: an experimental and modelling approach, Mec. Ind. 21 (2020) 605, https://doi.org/10.1051/MECA/2020078.
[88] L. Zhang, T. Hashimoto, J. Yan, Machinability exploration for high-entropy alloy FeCrCoMnNi by ultrasonic vibration-assisted diamond turning, CIRP Ann 70 (2021) 37–40, https://doi.org/10.1016/J.CIRP.2021.04.090.
[89] J. Yan, T. Okuuchi, Chip morphology and surface integrity in ultraprecision cutting of yttria-stabilized tetragonal zirconia polycrystal, CIRP Ann 68 (2019) 53–56, https://doi.org/10.1016/J.CIRP.2019.04.050.
[90] S. Gao, Y. Wu, R. Kang, H. Huang, Nanogrinding induced surface and deformation mechanism of single crystal β-Ga2O3, Mater. Sci. Semicond. Process. 79 (2018) 165–170, https://doi.org/10.1016/J.MSSP.2017.12.017.

[91] Y. Kakinuma, S. Azami, T. Tanabe, Evaluation of subsurface damage caused by ultra-precision turning in fabrication of CaF2 optical micro resonator, CIRP Ann 64 (2015) 117–120, https://doi.org/10.1016/J.CIRP.2015.04.076.
[92] W. Huang, J. Yan, Surface formation mechanism in ultraprecision diamond turning of coarse-grained polycrystalline ZnSe, Int. J. Mach. Tool Manufact. 153 (2020), 103554, https://doi.org/10.1016/J.IJMACHTOOLS.2020.103554.
[93] Z. Zhang, Y. Song, F. Huo, D. Guo, Nanoscale material removal mechanism of soft-brittle HgCdTe single crystals under nanogrinding by ultrafine diamond grits, Tribol. Lett. 46 (2012) 95–100, https://doi.org/10.1007/S11249-012-9924-9/FIGURES/4.
[94] A.W. Warren, Y.B. Guo, M.L. Weaver, The influence of machining induced residual stress and phase transformation on the measurement of subsurface mechanical behavior using nanoindentation, Surf. Coating. Technol. 200 (2006) 3459–3467, https://doi.org/10.1016/J.SURFCOAT.2004.12.028.
[95] J. Yan, H. Takahashi, J. Tamaki, X. Gai, H. Harada, J. Patten, Nanoindentation tests on diamond-machined silicon wafers, Appl. Phys. Lett. 86 (2005), 181913, https://doi.org/10.1063/1.1924895.
[96] K. Kosai, J. Yan, Effects of cyclic loading on subsurface microstructural changes of zirconia polycrystals in nanoscale mechanical processing, Int. J. Mach. Tool Manufact. 159 (2020), 103626, https://doi.org/10.1016/J.IJMACHTOOLS.2020.103626.
[97] J. Yan, H. Takahashi, X. Gai, H. Harada, J. Tamaki, T. Kuriyagawa, Load effects on the phase transformation of single-crystal silicon during nanoindentation tests, Mater. Sci. Eng. 423 (2006) 19–23, https://doi.org/10.1016/J.MSEA.2005.09.120.
[98] J. Yan, H. Takahashi, J. Tamaki, X. Gai, T. Kuriyagawa, Transmission electron microscopic observation of nanoindentations made on ductile-machined silicon wafers, Appl. Phys. Lett. 87 (2005), 211901, https://doi.org/10.1063/1.2133908.
[99] H.H. Yueqin Wu, Qijian Rao, James P. Best, Dekui Mu, Xipeng Xu, Superior room temperature compressive plasticity of submicron beta-phase gallium oxide single crystals, Adv. Funct. Mater. 2207960 (2022), https://doi.org/10.1002/adfm.202207960.
[100] 15 (n.d.), https://alemnis.com/micropillar-compression/.
[101] Z. Liao, D. Axinte, M. Mieszala, R. M' Saoubi, J. Michler, M. Hardy, On the Influence of Gamma Prime upon Machining of Advanced Nickel Based Superalloy, CIRP Ann, 2018.
[102] R. Ding, C. Knaggs, H. Li, Y.G. Li, P. Bowen, Characterization of plastic deformation induced by machining in a Ni-based superalloy, Mater. Sci. Eng., A (2020), 139104.
[103] B. Medina-Clavijo, J. Rafael-Velayarce, E. Modin, M. Saez-de-Buruaga, D. Soler, C. Motz, P.J. Arrazola, A. Chuvilin, Mechanical Properties of Friction Induced Nanocrystalline Pearlitic Steel, 2022.
[104] Z. Liao, M. Polyakov, O.G. Diaz, D. Axinte, G. Mohanty, X. Maeder, J. Michler, M. Hardy, Grain refinement mechanism of nickel-based superalloy by severe plastic deformation - mechanical machining case, Acta Mater. 180 (2019) 2–14, https://doi.org/10.1016/j.actamat.2019.08.059.
[105] J.A. Robles-Linares, D. Axinte, Z. Liao, A. Gameros, Machining-induced thermal damage in cortical bone: necrosis and micro-mechanical integrity, Mater. Des. 197 (2021), 109215.
[106] Y. Zhang, J.A. Robles-Linares, L. Chen, Z. Liao, A.J. Shih, C. Wang, Advances in machining of hard tissues–From material removal mechanisms to tooling solutions, Int. J. Mach. Tool Manufact. 172 (2022), 103838.
[107] C. Liu, W. Lu, W. Xia, C. Du, Z. Rao, J.P. Best, S. Brinckmann, J. Lu, B. Gault, G. Dehm, G. Wu, Z. Li, D. Raabe, Massive interstitial solid solution alloys achieve near-theoretical strength, Nat. Commun. 13 (2022) 1–9, https://doi.org/10.1038/s41467-022-28706-w.